THE JOURNAL OF PHYSICAL CHEMISTRY C
A JOURNAL OF THE AMERICAN CHEMICAL SOCIETY

pubs.acs.org/JPCC

Article

Understanding the Local Structure, Magnetism, and Optical Properties in Layered Compounds with d^9 Ions: Insight into Silver Fluorides and K_2CuF_4

Published as part of The Journal of Physical Chemistry C virtual special issue "The Physical Chemistry of Perovskites".

Inés Sánchez-Movellán, Guillermo Santamaría-Fernández, Pablo García-Fernández, José Antonio Aramburu,* and Miguel Moreno

Cite This: *J. Phys. Chem. C* 2023, 127, 16695−16708

Read Online

ACCESS | Metrics & More | Article Recommendations

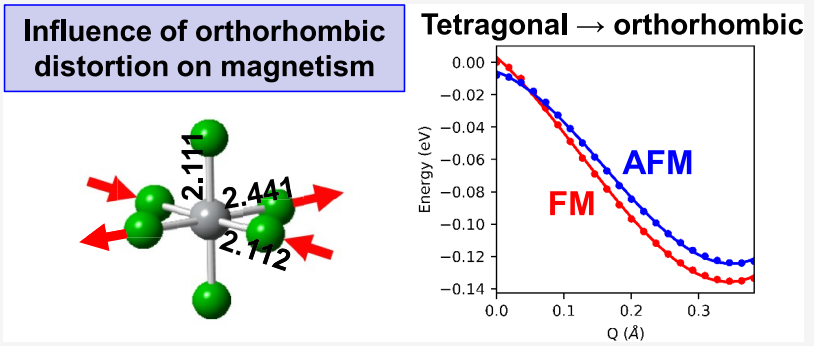

ABSTRACT: Using first-principles density functional theory calculations, we analyze the origin of the different crystal structures and optical and magnetic properties of two basic families of layered fluoride materials with the formula A_2MF_4 (M = Ag, Cu, Ni, and Mn; A = K, Cs, and Rb). On one hand, Cs_2AgF_4 and K_2CuF_4 compounds (both with d^9 metal cations) crystallize in an orthorhombic structure with the *Cmca* space group and M_A-F-M_B bridge angle of 180°, and they exhibit a weak ferromagnetism (FM) in the layer plane. On the other hand, K_2NiF_4 or K_2MnF_4 compounds (with d^8 and d^5 metal cations, respectively) have a tetragonal *I4/mmm* space group with a 180° bridge angle and exhibit antiferromagnetism (AFM) in the layer plane. First, we show that, contrary to what is claimed in the literature, the *Cmca* structure of Cs_2AgF_4 and K_2CuF_4 is not related to a cooperative Jahn−Teller effect among elongated MF_6^{4-} units. Instead, first-principles calculations carried out in the *I4/mmm* parent phase of these two compounds show that MF_6^{4-} units are axially compressed because the electrostatic potential from the rest of the lattice ions forces the hole to lie in the $3z^2-r^2$ molecular orbital (z being perpendicular to the layer plane). This fact increases the metal−ligand distance in the layer plane and makes that the covalency in the bridging ligand have a residual character (clearly smaller than in K_2NiF_4 or $KNiF_3$) stabilizing for only a few meV (7.9 meV for Cs_2AgF_4), an AFM order. However, this *I4/mmm* parent phase of Cs_2AgF_4 is unstable, thus evolving toward the experimental *Cmca* structure with an energy gain of 140 meV, FM ordering, and orthorhombic MF_6^{4-} units. As a salient feature, it is shown that the FM order in Cs_2AgF_4 and K_2CuF_4 is due to the asymmetry of the in-plane M_A-F-M_B bridge, giving rise to a negligible covalency for the long bond. Moreover, in K_2NiF_4 or K_2MnF_4, the lack of excited states within the d^n manifold (n = 8 and 5) of M, which can be coupled to the ground state for a local b_{1g} distortion mode, hampers the orthorhombic instability, thus favoring the AFM ordering. The present ideas also account for the experimental optical and EPR data of Cs_2AgF_4 and K_2CuF_4. An additional discussion on the silver compound Rb_2AgF_4 is also reported.

1. INTRODUCTION

In the realm of insulating layered perovskites,[1,2] much research is currently focused on those containing the $3d^9$ ion Cu^{2+} due to their attractive optical and magnetic properties.[3−6] Inorganic compounds[7−12] like K_2CuF_4 or Rb_2CuCl_4 as well as organic−inorganic hybrid perovskites of the $(C_nH_{2n+1}NH_3)_2CuCl_4$ or $[NH_3(CH_2)_nNH_3]CuX_4$ (X = Cl and Br) families[13−16] belong

Received: June 9, 2023
Revised: July 31, 2023
Published: August 15, 2023

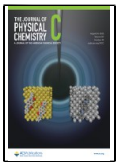

to these kinds of materials. In all these insulating transition-metal compounds, properties are greatly dependent on the equilibrium geometry and the related electronic structure of the CuX_6^{4-} complex (X = F, Cl, and Br) formed in the crystal.

In the last two decades, significant efforts have been focused to exploring insulating compounds that contain the $4d^9$ ion, Ag^{2+}, partially driven by the search of new superconducting materials.[17] As the optical electronegativity[18] of Ag^{2+} ($\chi = 2.8$) is higher than that of Cu^{2+} ($\chi = 2.4$) and identical to that of the Br^- ion,[19] only crystals of silver(II) fluorides have been synthesized up to now. In chloride and bromide lattices, Ag^{2+} has been found only as impurity. For instance, Ag^{2+} has been formed in alkali chlorides[20−22] and $SrCl_2$[20−22] while the $AgBr_6^{4-}$ complex has been observed in $CdBr_2$:Ag^{2+}[23] and $AgBr_{0.15}Cl_{0.85}$:Ag^{2+}[24] where the hole is mainly placed on ligands and not on the central cation.[18,22]

Silver compounds of the series A_2AgF_4 (A = Cs and Rb) display a layered structure with Cs_2AgF_4 as the most studied compound up to now.[25−36] From the first X-ray measurements, Odenthal et al. initially proposed[25] a tetragonal layered structure like that of K_2NiF_4 (space group *I4/mmm*) for Cs_2AgF_4. However, accurate neutron diffraction data by McLain et al. proved[28] that Cs_2AgF_4 is actually orthorhombic (space group *Cmca*), thus displaying the same crystal structure as K_2CuF_4.

In many previous works, the local geometry and electronic ground state of AgF_6^{4-}units in Cs_2AgF_4 have been assumed to be the result of a Jahn−Teller (JT) effect and/or orbital ordering.[26−36] Nonetheless, the existence of a JT effect in Cs_2AgF_4 is hard to accept as the lattice is orthorhombic while doubts were already raised[11] on the orbital ordering as responsible for the structure of both K_2CuF_4 and La_2CuO_4. Moreover, we believe that the existence of a small ferromagnetic (FM) coupling in the layer plane of Cs_2AgF_4 and K_2CuF_4 has not been explained in a clear and convincing way. For example, no compelling reasons have been proposed to explain why the transition temperature, T_c, observed for both Cs_2AgF_4 (15 K)[28] and K_2CuF_4 (6.25 K),[7] is certainly smaller than that for the tetragonal perovskite K_2NiF_4 (97.3 K) or the cubic perovskite $KNiF_3$ (246 K), which are both antiferromagnetic[37,38] (AFM).

This work is first devoted to clearing up the origin of the equilibrium geometry and electronic ground state of AgF_6^{4-} units in A_2AgF_4 (A = Cs and Rb) compounds paying special attention to Cs_2AgF_4. To achieve this goal, first-principles calculations together with an analysis of available experimental data are carried out. Once this key issue is clarified, we further discuss the origin of the FM ordering in the layer plane of Cs_2AgF_4 observed below T_c = 15 K.

Interestingly, we try to verify in this work whether some new ideas used for understanding copper layered compounds[11,12,39] are also valid for the present case. Accordingly, we first focus on the *I4/mmm* parent phase of Cs_2AgF_4 paying attention to the internal electric field, $\mathbf{E}_R(\mathbf{r})$, due to the rest of the lattice ions on the behavior of the AgF_6^{4-} unit where active electrons are confined. This internal field plays a key role for understanding the color of Cr^{3+} gemstones[22,40] or the ground state[41,42] of CuF_6^{4-}units in K_2ZnF_4:Cu^{2+}. For this reason, we explore here the influence of $\mathbf{E}_R(\mathbf{r})$ on the nature of the electronic ground state of AgF_6^{4-} complexes in Cs_2AgF_4 and the associated metal−ligand distances. If the parent phase's structure is different from the equilibrium geometry of Cs_2AgF_4, then it implies the existence of an instability[12] discussed in a second step.

Available electron paramagnetic resonance (EPR) and optical data of Rb_2AgF_4 are quite close[26,43,44] to those found for Cs_2AgF_4, thus suggesting that Rb_2AgF_4 also exhibits a *Cmca* structure, a matter also analyzed in the present work.

This work is organized as follows: Section 2 provides a detailed explanation of the computational tools employed. In Section 3.1, an overlook on previous interpretations of structural, optical, and magnetic data of layered silver fluorides is presented, while the remaining part of Section 3 displays the main results obtained for Cs_2AgF_4 and K_2CuF_4. As Cs_2AgF_4 and K_2CuF_4 are model systems in the realm of layered compounds, Section 3 is devoted to improving the knowledge on the structural (Section 3.2), EPR (Section 3.3), and optical data (Section 3.4) of both compounds as well as discussing the origin of their FM behavior not observed in K_2NiF_4 or K_2MnF_4 (Section 3.5). Additionally, Section 3.6 briefly discusses the main results obtained in Rb_2AgF_4. Finally, some conclusions are provided in Section 4.

2. COMPUTATIONAL TOOLS

First-principles calculations based on Kohn−Sham density functional theory (DFT)[45] were performed on pure K_2CuF_4, Cs_2AgF_4, Cs_2CdF_4, Rb_2AgF_4, and K_2NiF_4. To carry out periodic calculations, the Crystal17 package was used.[46,47] This software makes a full use of the crystal symmetry, allowing us to perform geometry optimizations within specific space groups. In this sense, we can compute unstable phases, such as the high-symmetry parent phases of these compounds, which cannot experimentally be measured.[11,12,48−50] The instabilities occurring in these phases were explored through frequency calculations considering both FM and AFM orders, as discussed in Section 3.5.

In Crystal 17 code, Bloch wavefunctions are represented by linear combinations of Gaussian-type basis functions[51,52] centered at atomic sites. The basis sets for the ions were taken from Crystal's webpage.[52] High-quality triple-zeta polarized basis developed by Peitinger et al. was employed.[51] For heavy ions (Ag^{2+}, Cd^{2+}, and Cs^+), pseudopotentials were used to describe the inner electrons. The exchange-correlation functional employed in these calculations was the hybrid PW1PW, which incorporates 20% of Hartree−Fock (HF) exact exchange. This functional has been proven to yield accurate results for the geometry and properties of several pure and doped systems.[53] The obtained results were also cross-verified with another hybrid functional (B1WC) including 16% of HF exchange and different basis sets, leading to similar outcomes.

To ensure convergence, tight criteria were imposed for energy variations (10^{-9} a.u.) as well as for root mean square (RMS) gradients and atomic displacement (0.0001 a.u.). A Monkhorst−Pack grid of 8 × 8 × 8 was used to sample the Brillouin zone for numerical integrations.

In addition to periodic calculations, cluster simulations were performed using the ADF software.[54] The hybrid B3LYP functional, which incorporates 25% of HF exchange, together with triple-zeta polarized basis sets, was used in the calculations. The core electrons were kept frozen as they do not significantly influence the properties under study. These calculations make it possible to explore the optical spectra of both isolated and embedded complexes by just considering[11,12,39,55,56] the potential created by the rest of the lattice

https://doi.org/10.1021/acs.jpcc.3c03895
J. Phys. Chem. C 2023, 127, 16695−16708

ions V_R. The electrostatic potential, particularly relevant in layered systems, was previously computed by Ewald−Evjen summations.[57,58] As shown in Section 3.4, we can reproduce the experimental optical d−d transitions for CuF_6^{4-} and AgF_6^{4-} with reasonable accuracy when including the electrostatic potential V_R. Despite apparent differences in d−d transitions of these two systems, we demonstrate their consistent behavior. Furthermore, our calculations on complexes provided valuable information about hybridization and covalency parameters of molecular orbitals, which are closely associated with the exchange constant J, as discussed in Section 3.5.

3. RESULTS AND DISCUSSION ON Cs_2AgF_4 AND K_2CuF_4

3.1. Survey of Previous Works on Layered Silver Fluorides. According to the results by McLain et al., Cs_2AgF_4 is a layered compound belonging to the orthorhombic *Cmca* space group,[28] with **a** as the crystal axis perpendicular to the layer plane (Figure 1). The experimental values of lattice

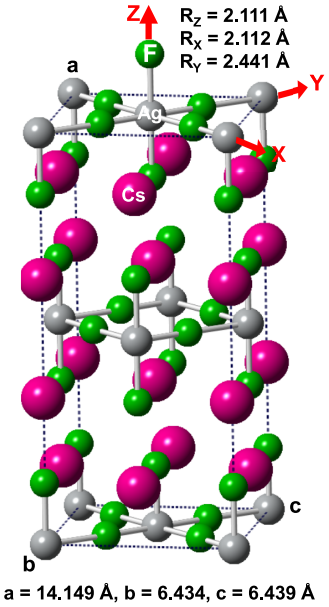

Figure 1. Experimental *Cmca* structure of Cs_2AgF_4 displaying the local $\{X,Y,Z\}$ axes of a orthorhombic AgF_6^{4-} unit. Values of the lattice parameters and the three Ag^{2+}−F^- bond distances are shown.

parameters and Ag−F distances are also shown in Figure 1. R_Z = 2.111 Å corresponds to the Ag−F direction perpendicular to the layer plane, while R_X = 2.112 Å and R_Y = 2.441 Å are associated, respectively, with the short and long Ag−F distances within the layer plane.

Cs_2AgF_4 exhibits an antiferrodistortive arrangement, and thus, if we move along the line joining the two nearest Ag^{2+}, then the local longest y axes of two involved AgF_6^{4-} units are perpendicular (Figure 2). Interestingly, there is a weak FM exchange coupling, H_{ex}, between the two nearest cations (with spins $\mathbf{S}_1$ and $\mathbf{S}_2$) in the layer plane of Cs_2AgF_4 described through the effective exchange interaction

$$H_{ex} = J\ \mathbf{S}_1 \cdot \mathbf{S}_2 \tag{1}$$

with J = −3.79 meV.[28] This situation, also found in K_2CuF_4,[7,28] is somewhat surprising as in layered compounds like K_2NiF_4 or

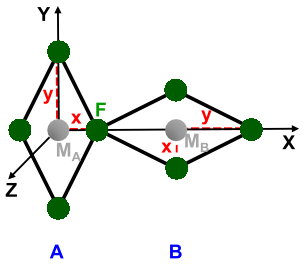

Figure 2. Schematic view of the in-plane antiferrodistortive arrangement of two adjacent A and B AgF_6^{4-}units in Cs_2AgF_4, where the two local longest y axes are perpendicular.

K_2MnF_4, the coupling between magnetic cations in the layer plane is AFM.[38]

Concerning the EPR spectra of Cs_2AgF_4 in powder, two peaks are well observed.[26,43] One signal, $g(\mathbf{a})$, corresponds to the magnetic field **B** parallel to the **a** axis while $g(\perp\mathbf{a})$ is the gyromagnetic factor when **B** lies in the layer plane. This isotropic response when **B** is in the layer plane obeys to the exchange interaction[59] between two nearest complexes, A and B. Indeed, using the local $\{x,y,z\}$ bases of A and B complexes in Figure 2, the $g(i)$ (i = A and B) tensors in the crystal $\{X,Y,Z\}$ basis are given by

$$g(\mathrm{A}) = \begin{pmatrix} g_y & 0 & 0 \\ 0 & g_x & 0 \\ 0 & 0 & g_z \end{pmatrix} \qquad g(\mathrm{B}) = \begin{pmatrix} g_x & 0 & 0 \\ 0 & g_y & 0 \\ 0 & 0 & g_z \end{pmatrix} \tag{2}$$

Nevertheless, when the interaction of **B** with $\mathbf{S}_1$ or $\mathbf{S}_2$ is much smaller than H_{ex}, the phenomenon of exchange narrowing takes place[59] and then $g(\perp\mathbf{a})$ is just given by

$$g(\perp\mathbf{a}) = (g_x + g_y)/2 \tag{3}$$

If J = −3.79 meV, then the condition $|J| \gg \mu_B B$ (μ_B is the Bohr magneton) is well fulfilled working in the Q band (B = 1.2 T) or even using B = 10 T.[26]

The local geometry around Ag^{2+} in Cs_2AgF_4 has widely been assumed to arise from a JT effect leading to elongated tetragonal AgF_6^{4-} units[26,28,30,33,35,43] with y as the local principal axis of the complex and the hole placed in a molecular orbital transforming like z^2-x^2. To underpin this view, McLain et al. argue[28] that for JT complexes of d^9 ions, the hole is always placed in an orbital of the type x^2-y^2. Accepting the JT assumption, the experimental $g(\mathbf{a}) = g_z$ value should then correspond to the $g_\perp$ quantity characteristic of a tetragonal complex while $g_y = g_\parallel$ and $g_x = g_\perp$. Therefore, in that case, $g(\perp\mathbf{a})$ should be equal to

$$g(\perp\mathbf{a}) = (g_\perp + g_\parallel)/2 \tag{4}$$

Nonetheless, doubts are raised by the JT assumption due to the following reasons:

(i) The existence of a JT effect requires a degenerate electronic state in the initial geometry.[60−62] Even if that parent geometry corresponds to a *I*4/*mmm* tetragonal phase, the electronic ground state of a AgF_6^{4-} unit should not be degenerate due to symmetry reasons.

(ii) Cs_2AgF_4 is a layered compound where layers are perpendicular to the **a** crystal axis. Therefore, it is surprising that under the JT assumption, the principal

https://doi.org/10.1021/acs.jpcc.3c03895
J. Phys. Chem. C 2023, 127, 16695−16708

Table 1. Calculated Values of Lattice Parameters and Distances for Cs_2AgF_4[a]

step	compound	space group	a	b	c	R_z	R_x	R_y
(1)	Cs_2CdF_4	*Cmca*	14.773	6.392	6.392	2.216	2.260	2.260
(2)	Cs_2AgF_4	*I4/mmm*	4.585	4.585	14.238	2.081	2.292	2.292
(3)	Cs_2AgF_4	*Cmca*	14.382	6.454	6.455	2.130	2.106	2.458
experim.	Cs_2AgF_4	*Cmca*	14.149	6.434	6.439	2.112	2.111	2.441

[a]Step (1): calculated values of lattice parameters and Cd−F distances for Cs_2CdF_4 assuming an initial *Cmca* structure, which is the equilibrium structure of Cs_2AgF_4. It evolves until it reaches an equilibrium tetragonal *I4/mmm* structure where $b = c$ and $R_x = R_y$. Step (2): calculated lattice parameters and Ag−F distances corresponding to Cs_2AgF_4 but fixing a *I4/mmm* space group. Step (3): Idem that step (2) but derived for the *Cmca* equilibrium structure. The last values are compared to the experimental ones.[28] Note that the *c* axis in the standard *I4/mmm* becomes the *a* axis in the standard *Cmca*. All distances are given in Å units.

axis of the AgF_6^{4-} unit is in the layer plane and not perpendicular to it.

(iii) The local equilibrium geometry for AgF_6^{4-} in Cs_2AgF_4 is not tetragonal but orthorhombic, although R_Z and R_X are very close, as shown in Figure 1.

(iv) From eq 4 and the experimental values $g(\mathbf{a}) = 2.07$ and $g(\perp\mathbf{a}) = 2.25$, we get $g_{\parallel} - g_0 = 0.42$ and $g_{\perp} - g_0 = 0.07$, which are rather different from $g_{\parallel} - g_0 = 0.57$ and $g_{\perp} - g_0 = 0.11$ measured for the cubic lattice $CsCdF_3$ doped with Ag^{2+}, where EPR data prove the existence of a static JT effect with elongated AgF_6^{4-} units.[63]

(v) Optical spectra on Cs_2AgF_4 and Rb_2AgF_4 by Friebel and Reinen in the range of 0.5−3.5 eV suggest the existence of four and not three d−d transitions,[43] a fact consistent with a local orthorhombic symmetry around Ag^{2+}. However, in the case of K_2CuF_4, which also displays a *Cmca* structure, only three d−d transitions have been observed[10] even working at $T = 5$ K, a matter that is certainly puzzling.[64]

(vi) Although most of d^9 systems, which exhibit a static JT effect, are elongated with a hole in a x^2-y^2-type orbital,[21,60,62] this is not a general rule. For instance, in the cubic CaO lattice doped with Ni^+, the hole is in a $3z^2-r^2$ orbital and the octahedron is compressed.[65,66] In non-JT systems like $K_2ZnF_4:Cu^{2+}$, where the host lattice is tetragonal,[41,42] the hole is also in $3z^2-r^2$.

The following sections are addressed to clarify all these questions with the help of first-principles simulations.

3.2. Origin of the Structure and Electronic Ground State. To explain in a consistent way the experimental results on Cs_2AgF_4 exposed in Section 3.1, it is crucial to know the actual ground state of involved AgF_6^{4-} units and the origin of its equilibrium geometry. For achieving this goal, we have followed three steps:

(1) First, we have determined the parent phase of the *Cmca* structure of Cs_2AgF_4 by substituting all Ag^{2+} ions of Cs_2AgF_4 by the closed shell cation Cd^{2+}, with an ionic radius similar to that of Ag^{2+}, and performed a geometry optimization, keeping fixed the *Cmca* space group. As shown in Table 1, under the $Ag^{2+} \rightarrow Cd^{2+}$ substitution, the structure evolves from the initial orthorhombic to a final one where $a = b$ and $R_X = R_Y$, associated with a tetragonal *I4/mmm* symmetry. In this parent structure, $R_Z < R_X$, although $R_X - R_Z$ is equal only to 0.044 Å. This *I4/mmm* parent phase, characteristic of compounds like K_2NiF_4 or K_2ZnF_4, is the same previously found[11,12] in K_2CuF_4.

(2) Then, it is useful to explore the behavior of Cs_2AgF_4 fixing the *I4/mmm* structure of the parent phase. Interestingly, the results of step (2) (Table 1) show that in the *I4/mmm* structure, the AgF_6^{4-} units are tetragonally compressed ($R_z < R_x = R_y$) with a hole in the antibonding molecular orbital transforming like $3z^2-r^2$. Therefore, in this step, the principal axis of the AgF_6^{4-} unit is perpendicular to the layer plane. As it also happens[11,12,41,42] for $K_2ZnF_4:Cu^{2+}$ or K_2CuF_4, this ground state is helped by the action of the internal electric field $\mathbf{E}_R(\mathbf{r})$ on active electrons confined in the AgF_6^{4-} unit. Figure 3 depicts the energy of an electron (−e charge) of a AgF_6^{4-} unit under the electrostatic potential, $V_R(\mathbf{r})$, generating the internal electric field, $\mathbf{E}_R(\mathbf{r})$, through $\mathbf{E}_R(\mathbf{r}) = -\nabla V_R(\mathbf{r})$. It can be seen that $-eV_R(\mathbf{r})$ raises the energy of an electron placed in $3z^2-r^2$, while it lowers that of an x^2-y^2 electron; thus, this fact alone favors locating the hole in a $3z^2-r^2$ orbital. This behavior of the $-eV_R(\mathbf{r})$ energy is thus similar to that found in compounds like K_2BF_4 (B = Mg, Zn, and Cu), which also exhibits a layered structure.[11,12,41,42]

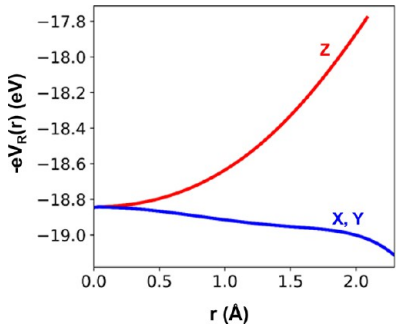

Figure 3. Potential energy $-eV_R(\mathbf{r})$ corresponding to the internal electric field created by the rest of the lattice ions on a AgF_6^{4-} unit of Cs_2AgF_4 in the tetragonal *I4/mmm* parent phase, depicted along the local *X*, *Y*, and *Z* directions of the complex.

It is worth noting that on passing from Cs_2CdF_4 to Cs_2AgF_4, keeping the *I4/mmm* structure, $R_x - R_z$ increases by a factor close to 5. This significant difference just reflects that Ag^{2+} does not have a closed shell[58] structure as Cd^{2+}. Indeed, in the tetragonal phase of Cs_2AgF_4, if there is a hole in the $3z^2-r^2$ orbital, then this induces[67] an attractive force on two axial ligands and an increase in $R_X - R_Z$. Due to this process, at the end of step (2), there are two Ag−F bonds with $R_Z = 2.081$ Å while four softer at a distance $R_x = R_y = 2.292$ Å.

(3) In a further step, when the *I4/mmm* restriction is lifted, the calculated structure of Cs_2AgF_4 evolves until reaching a *Cmca* space group. As shown in Table 1, the optimized lattice parameters and Ag−F distances in step (3) coincide with those measured experimentally within 1.6%.

It should be remarked that, on passing from step (2) to step (3), R_z undergoes a slight increase of 0.049 Å while $R_y - R_x$ moves from 0 to 0.35 Å, implying a significant distortion in the layer plane. This fact supports that the local equilibrium

https://doi.org/10.1021/acs.jpcc.3c03895
J. Phys. Chem. C 2023, 127, 16695−16708

geometry of the AgF_6^{4-} unit in step (3) is essentially orthorhombic, despite the experimental R_x and R_z values differing at the end by 0.001 Å (Table 1). Considering this fact alone, previous works on Cs_2AgF_4 have assumed[26,28,30,33,35,43] the existence of a JT effect with the local y as the principal axis. The same assumption has been applied[9,10,68] to explain K_2CuF_4 where experimental Cu^{2+}−F^- distances[8] are R_z = 1.939 Å, R_x = 1.941 Å, and R_y = 2.234 Å.

The nature of the electronic ground state of AgF_6^{4-} units derived from present calculations sheds light to clarify this key issue. Indeed, they reveal that the hole keeps a dominant $3z^2-r^2$ character at the equilibrium geometry of Cs_2AgF_4 (step (3)). More precisely, an orthorhombic distortion allows the admixture of the molecular orbitals $|3z^2-r^2\rangle$ and $|x^2-y^2\rangle$ of the AgF_6^{4-} unit for describing the wavefunction of the hole, $|\varphi_H\rangle$, and thus

$$|\varphi_H\rangle = \alpha|3z^2 - r^2\rangle - \beta|x^2 - y^2\rangle \quad (5)$$

The present calculations give β^2 = 19%, underlining that the orthorhombic distortion has only a moderate effect on $|\varphi_H\rangle$, a situation consistent with the degree of orthorhombicity given by the quantity $\eta = 2(R_y - R_x)/(R_y + R_x)$. Indeed, using the R_y and R_x values given in Table 3, we obtain η = 14.5%.

The results in Table 1 support that the parent phase $I4/mmm$ (where $R_y = R_x$) is not the stable one for Cs_2AgF_4. This instability is helped by the vibronic coupling between the electronic ground state of a AgF_6^{4-} unit, $^2A_{1g}$, and $^2B_{1g}$ excited states driven by a b_{1g} distortion mode described in Figure 4.

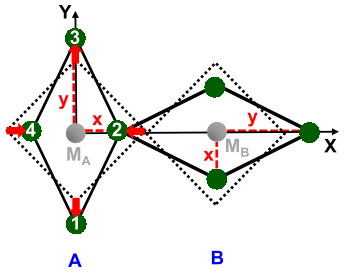

Figure 4. b_{1g} distortion mode of the four planar F^- ligands (red arrows) of a given AgF_6^{4-} unit of Cs_2AgF_4, going from a square to a rhombus where $R_y \neq R_x$. The b_{1g} distortion mode can be described in terms of the normal coordinate Q, given by $Q = \frac{1}{2}(-u_1 - u_2 + u_3 + u_4)$, where u_i ($u_1 = -u_3 = u_2 = -u_4$) are the displacements of atoms 1−4, respectively.

That coupling is symmetry-allowed and can lead to a total force constant that becomes negative ($K < 0$), thus favoring a *Cmca* phase at equilibrium. According to that distortion mode (Figure 4), the four planar F^- ligands of a given Ag^{2+} forming initially a square give rise at the end to a rhombus where $R_Y \neq R_X$.

To clarify this relevant matter, a negative force constant can take place as there are two contributions[69] to the force constant K. Let us designate by $H_0(\mathbf{r})$, the electronic Hamiltonian when the lattice is frozen at equilibrium positions. The corresponding ground state wavefunction is termed $\Psi_0(\mathbf{r})$, while excited states are $\Psi_i(\mathbf{r})$ with $i > 0$. If we move around the equilibrium position activating a Q coordinate, then a new vibronic term, $h(Q,\mathbf{r})$, has to be added to the Hamiltonian

$$H = H_0(\mathbf{r}) + h(Q, \mathbf{r}) \quad (6)$$

with $h(0,\mathbf{r}) = 0$. The first elastic contribution to the force constant, called K_0, comes from considering only $h(Q,\mathbf{r})$ and $\Psi_0(\mathbf{r})$, thus neglecting the changes on the ground state wavefunction caused by the Q distortion. However, the presence of $h(Q,\mathbf{r})$ also makes that the ground state wavefunction is no longer $\Psi_0(\mathbf{r})$ but involves an admixture of excited states $\Psi_i(\mathbf{r})$, giving rise to a negative vibronic contribution, K_v, to the force constant. If Q is a non-symmetric non-degenerate vibration mode transforming as irrep Γ, then $h(Q,\mathbf{r})$ is usually expanded as

$$h(Q, \mathbf{r}) = V(\mathbf{r})Q + \ldots \quad (7)$$

where, in the linear electron-vibration coupling, $V(\mathbf{r})$ transforms like Q. In second-order perturbation theory, this coupling gives rise to the following expression for K_v

$$K_v = -\sum_{i>0} \frac{|\langle\Psi_0|V(r)|\Psi_i\rangle|^2}{E_i - E_0} \quad (8)$$

Accordingly, $K_v < 0$ for the electronic ground state, and K is just given by[69]

$$K = K_0 - |K_v| \quad (9)$$

The excited states in eq 8 must have the same spin as the ground state. Moreover, if $\Psi_0(\mathbf{r})$ and $\Psi_i(\mathbf{r})$ belong to the irreps Γ_0 and Γ_i, respectively, then non-zero matrix elements in eq 8 are obtained only when $\Gamma_0 \otimes \Gamma_i \supset \Gamma$. Therefore, in a tetragonal MF_6^{4-} complex (M = Cu and Ag), a $^2A_{1g}$ ground state can be mixed with an excited $^2B_{1g}$ state, involving a hole in x^2-y^2, through the vibronic coupling involving a local b_{1g} distortion mode.[70]

According to eq 9, the instability develops when K becomes negative and is favored for low values of K_0 and thus soft bonds. If initially there is a compressed tetragonal complex, then $R_z < R_y = R_x$ and thus the equatorial bonds are softer than the axial ones. This fact favors in principle the development of an orthorhombic distortion in the equatorial plane,[11,12,39,67] provided that $K < 0$. On the contrary, when the complex is elongated and $R_z > R_y = R_x$, it hardens the equatorial bonds, a fact that works against the distortion. For this reason, in systems like $NaCl:M^{2+}$[20,21,71] or $CsCdF_3:M^{2+}$ (M = Cu and Ag)[49] where MX_6^{4-} units (X = Cl and F) are tetragonally elongated, no orthorhombic distortion in the equatorial plane has been observed. The same situation is encountered for La_2CuO_4.[11]

In the case of layered compounds, the condition $K < 0$ can be better fulfilled for chlorides than for fluorides where bonds are stronger. For this reason, the orthorhombic distortion in the layer plane has already been observed[72] for Cu^{2+}-doped $(CH_3NH_3)_2CdCl_4$ but not for $K_2ZnF_4:Cu^{2+}$ where CuF_6^{4-} units display a compressed tetragonal symmetry.[73] Nevertheless, if we move to the pure compound K_2CuF_4, two adjacent CuF_6^{4-}complexes share a common ligand and this fact has been shown[12] to help K to become negative. This situation is also found in Cs_2AgF_4.

3.3. Interpretation of EPR Data of Cs_2AgF_4 and K_2CuF_4.

The orthorhombic instability taking place in Cs_2AgF_4 obeys to the same grounds previously discussed[11,12] for K_2CuF_4. For this reason, we have now to reinterpret the EPR data obtained[26,43] for Cs_2AgF_4 based on AgF_6^{4-} units initially compressed along the z axis that undergo a moderate orthorhombic distortion (η = 14.5%) in the layer plane. For a compressed tetragonal AgF_6^{4-} unit, g_z differs from g_0 only in

https://doi.org/10.1021/acs.jpcc.3c03895
J. Phys. Chem. C 2023, 127, 16695−16708

Table 2. Calculated Energy Values (in eV) of Four d−d Transitions for a CuF_6^{4-} Unit in K_2CuF_4 at the Equilibrium *Cmca* Structure Where Experimental Cu^{2+}−F^- Distances Are R_z = 1.939 Å, R_x = 1.941 Å, and R_y = 2.234 Å[a]

	$x^2-y^2 \rightarrow 3z^2-r^2$	$xz \rightarrow 3z^2-r^2$	$yz \rightarrow 3z^2-r^2$	$xy \rightarrow 3z^2-r^2$
isolated CuF_6^{4-}	0.77	1.13	1.32	1.31
CuF_6^{4-} under $V_R(\mathbf{r})$	1.04	1.17	1.42	1.51
experimental	1.03	1.17	1.50	1.50

[a]For the sake of clarity, the transitions are first derived ignoring the internal potential $V_R(\mathbf{r})$, whereas its influence upon the CuF_6^{4-} unit is considered in a second step. Experimental values[10] for K_2CuF_4 are also reported for comparison. Due to the local orthorhombic symmetry of CuF_6^{4-} units in K_2CuF_4, a transition termed as $x^2-y^2 \rightarrow 3z^2-r^2$ only reflects the dominant character of involved orbitals.

third-order perturbations[74] and thus the tetragonal expression is

$$g_z(T) = g_0 - \Delta g^3 \tag{10}$$

For AgF_6^{4-}, the estimated third-order correction is $\Delta g^3 \approx 0.02$. In a further step, a moderate orthorhombicity induces an admixture of $|x^2-y^2\rangle$ in $|3z^2-r^2\rangle$ (eq 5), thus giving rise to a contribution to g_z in second-order perturbations). Accordingly, the octahedral expression of g_z in the equilibrium situation can be estimated by[39,70,74]

$$g_z(O) = g_0 - \Delta g^3 + \beta^2\, \delta g_z(x^2 - y^2) \tag{11}$$

Here, $\delta g_z(x^2-y^2) \equiv g_z(x^2-y^2) - g_0$ corresponds to a hole fully located in a pure $|x^2-y^2\rangle$ orbital. Taking $\delta g_z(x^2-y^2) \approx 0.55$ from EPR data[49] of $CsCdF_3$:Ag^{2+} and β^2 = 19% from present calculations for Cs_2AgF_4, we finally obtain $g_z(O)$ = 2.086, a figure reasonably close to the experimental value[26] g_z = 2.077.

Although for a compressed tetragonal AgF_6^{4-} unit with z as the main axis $g_y = g_x = g_\perp(T)$, the orthorhombic distortion in the layer plane leads finally to $g_y(O) \neq g_x(O)$. As the orthorhombicity is moderate (η = 14.5%), the difference between $g_y(O)$ and $g_x(O)$ comes mainly from the hybridization of $|3z^2-r^2\rangle$ and $|x^2-y^2\rangle$ (eq 5). In this case, the expressions of $g_y(O)$ and $g_x(O)$ are[39,70,74]

$$g_y(O) - g_0 = [g_\perp(T) - g_0]\left[1 + \frac{\beta}{\sqrt{3}}\right]^2$$

$$g_x(O) - g_0 = [g_\perp(T) - g_0]\left[1 - \frac{\beta}{\sqrt{3}}\right]^2 \tag{12}$$

Therefore, $g_y(O) - g_x(O)$ is given by

$$g_y(O) - g_x(O) = \frac{4\beta}{\sqrt{3}}[g_\perp(T) - g_0] \tag{13}$$

Due to the phenomenon of exchange narrowing,[45] when the magnetic field is in the layer plane of Cs_2AgF_4, only an isotropic signal $g(\perp\mathbf{a}) = (1/2)[g_x(O) + g_y(O)]$ is observed. From eq 12, that quantity can be expressed as follows

$$\frac{g_x(O) + g_y(O)}{2} - g_0 = [g_\perp(T) - g_0]\left[1 + \frac{\beta^2}{9}\right] \tag{14}$$

Therefore, from the experimental value[26,43] $g(\perp\mathbf{a})$ = 2.25 and the calculated β^2 = 19%, we derive from eqs 13 and 14 the values $g_y(O)$ = 2.38 and $g_x(O)$ = 2.12, respectively.

It is worth noting now that a similar situation is encountered in the layered compound K_2CuF_4 where experimental EPR data[7] yield $g(\mathbf{a})$ = 2.08 and $g(\perp\mathbf{a})$ = 2.30, while a value β^2 = 17% is obtained from calculations.[11] Interestingly, in the layered hybrid perovskite $(CH_3NH_3)_2CdCl_4$ doped with Cu^{2+}, there is also an orthorhombic distortion giving rise to the experimental values,[72,12] measured at T = 10 K, g_z = 2.05, g_y = 2.33, and g_x = 2.12. This pattern is thus comparable to that estimated for Cs_2AgF_4. The fingerprint of the orthorhombic instability in the chlorine plane is also found in NH_4Cl containing the $CuCl_4(H_2O)_2^{2-}$ radical where EPR data[75] at T = 4.2 K yield g_z = 2.02, g_y = 2.41, and g_x = 2.18. Obviously, in these cases involving impurities, there is no exchange narrowing but the average signal at $(1/2)(g_x + g_y)$ is also well seen upon raising the temperature due to a motional narrowing process.[74,20,21,48]

3.4. Interpretation of Optical Data of Cs_2AgF_4 and K_2CuF_4.

Concerning optical spectra, it is first necessary to understand why only three d−d transitions[10] have been reported experimentally for K_2CuF_4 while four[43] for Cs_2AgF_4, despite both compounds exhibiting the same *Cmca* structure.

The calculated d−d transitions for K_2CuF_4 at equilibrium are gathered in Table 2. These results first show the importance of considering the effect of the internal electric field $\mathbf{E}_R(\mathbf{r})$ on the electrons confined in the CuF_6^{4-} unit, where the shape[12] of the associated electrostatic potential, $V_R(\mathbf{r})$, is similar to that depicted in Figure 3 for a AgF_6^{4-} unit in Cs_2AgF_4. Once $V_R(\mathbf{r})$ is incorporated into the calculation, the two lowest d−d transitions essentially coincide with those observed experimentally[10] (Table 2). Interestingly, the present calculations for K_2CuF_4 reveal that there are four different transitions, although the two highest ones derived at 1.42 and 1.51 eV are only separated by 0.09 eV. The comparison of this figure with the bandwidth (∼0.30 eV) measured at T = 5 K of the band peaked at 1.50 eV reasonably explains why the two highest d−d transitions are not resolved in the optical spectrum of K_2CuF_4, in agreement with a previous work.[50]

Experimental optical data for Cs_2AgF_4 are collected in Table 3 together with the results of present calculations. As shown in Table 3, calculated d−d transitions follow the experimental pattern, but in this case, they underestimate the experimental energies by ∼0.2 eV. Again, the results gathered in Table 3 stress the significant role played by the internal field $\mathbf{E}_R(\mathbf{r})$, especially for understanding the value of the lowest $x^2-y^2 \rightarrow 3z^2-r^2$ transition and the 0.2 eV gap between the $yz \rightarrow 3z^2-r^2$ and $xy \rightarrow 3z^2-r^2$ transitions. At variance with what happens for K_2CuF_4, the existence of such a gap can well be inferred looking at the optical spectrum[43] of Cs_2AgF_4.

In view of the method followed for clarifying the structure of Cs_2AgF_4 in Section 3.2, it is worth analyzing the evolution of d−d transitions on passing from the *I*4/*mmm* parent phase to the equilibrium *Cmca* and the influence that the internal field, $\mathbf{E}_R(\mathbf{r})$, has upon them.[50,57] Results of present calculations are displayed in Figure 5. In the initial *I*4/*mmm* phase, ignoring $\mathbf{E}_R(\mathbf{r})$, the calculated d−d transitions are consistent with a local compressed tetragonal symmetry of the AgF_6^{4-} unit with z as the main axis. Accordingly, the $xz \rightarrow 3z^2-r^2$ and $yz \rightarrow 3z^2-r^2$

https://doi.org/10.1021/acs.jpcc.3c03895
J. Phys. Chem. C 2023, 127, 16695−16708

Table 3. Experimental d−d Transitions for Cs_2AgF_4 Compared to Those Derived from Present Calculations[a]

		$x^2-y^2 \rightarrow 3z^2-r^2$	$xz \rightarrow 3z^2-r^2$	$yz \rightarrow 3z^2-r^2$	$xy \rightarrow 3z^2-r^2$	CT
experimental	Friebel et al.[43]	1.59	1.92	2.27	2.45	
	Tong et al.[44]		1.91		2.48	4.59
calculated	Isolated AgF_6^{4-}	1.03	1.70	1.94	1.94	5.0
	AgF_6^{4-} with $V_R(\mathbf{r})$	1.43	1.74	1.97	2.18	4.94

[a]The transitions are first calculated ignoring the $V_R(\mathbf{r})$ potential, while its influence upon the AgF_6^{4-} unit is considered in a second step. Due to the local orthorhombic symmetry of AgF_6^{4-} units in Cs_2AgF_4, a transition termed as $x^2-y^2 \rightarrow 3z^2-r^2$ only reflects the dominant character of involved orbitals. The energy of the charge transfer (CT) transition observed[44] by Tong et al. is also given and compared to the calculated value. Transition energies are given in eV.

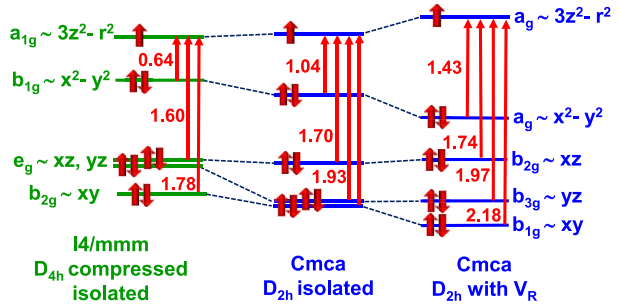

Figure 5. Evolution of mainly d orbitals of a AgF_6^{4-} unit of Cs_2AgF_4 and the corresponding d−d transitions (given in eV units) along the three steps. Left: isolated complex with the tetragonally compressed geometry (D_{4h} symmetry with $R_y = R_x > R_z$) optimized for the metastable *I4/mmm* parent phase. Center: isolated complex with the orthorhombic geometry (D_{2h} symmetry with $R_y \neq R_x$) optimized in the *Cmca* equilibrium structure. Right: the same geometry compared to the previous step but adding the effect of the internal electrostatic potential $V_R(\mathbf{r})$.

transitions are degenerate and the highest d−d transition is $xy \rightarrow 3z^2-r^2$. The local orthorhombic distortion associated with the *I4/mmm* → *Cmca* step increases significantly the gap between mainly $3z^2-r^2$ and x^2-y^2 levels from 0.64 to 1.03 eV as a result of the repulsion of these orbitals, both belonging to the a_g irrep under D_{2h} symmetry. At the same time, as the distortion makes that R_y becomes the longest metal−ligand distance, the energy of two levels *yz* and *xy* decreases and the $yz \rightarrow 3z^2-r^2$ and $xy \rightarrow 3z^2-r^2$ transitions are found to be accidentally degenerate. Finally, the inclusion of the $V_R(\mathbf{r})$ potential tends to increase the energy along the *z* direction (Figure 3). For this reason, it also enhances the energy of the transition between mainly the x^2-y^2 and $3z^2-r^2$ orbitals that move from 1.03 to 1.43 eV. In the same vein, the $xy \rightarrow 3z^2-r^2$ transition increases from 1.94 to 2.18 eV. Accordingly, the transition is no longer degenerate with $yz \rightarrow 3z^2-r^2$, nearly insensitive to the effects of $V_R(\mathbf{r})$.

The measurements[44] by Tong et al. on Cs_2AgF_4 also show a band peaked at 4.6 eV ascribed to a charge transfer transition of the AgF_6^{4-} unit. In the case of fluoride complexes, a charge transfer excitation in the optical range (up to 6.2 eV) cannot usually be observed due to the high electronegativity of fluorine (χ = 3.9). This hindrance however disappears for AgF_6^{4-} complexes[76] due to the high optical electronegativity of Ag^{2+} (χ = 2.8). Interestingly, in the case of the layered $(C_2H_5NH_3)_2CdCl_4$ compound doped with Cu^{2+}, the first allowed charge transfer transition is observed at 3.1 eV[5]. Thus, according to the optical electronegativities[19] of chlorine (χ = 3.0) and Cu^{2+} (χ = 2.4), we can estimate that such a transition would occur around 4.9 eV for Cs_2AgF_4. Our calculations (Table 3) lead to a transition energy equal to 4.95 eV.

3.5. Insight into the Ferromagnetism of Cs_2AgF_4 and K_2CuF_4 and Comparison with K_2NiF_4. This section addresses the origin of the two significant differences between the magnetic behavior of layered compounds Cs_2AgF_4 and K_2CuF_4 and that of the model system K_2NiF_4.

The main magnetic mechanism in play in these insulating lattices is superexchange that usually favors AFM ordering when the metal−ligand−metal bond occurs along a straight line. The main model describing superexchange, Anderson's model,[77−79] is usually applied in a straightforward manner to K_2NiF_4. However, systems containing d^9 ions, like Cs_2AgF_4 and K_2CuF_4, are usually said to contain an orbital degree of freedom, i.e., the energy of the system and magnetic ordering are heavily influenced by how the occupied orbitals orient with respect to each other. Kugel and Khomskiĭ proposed[80] the orbital ordering model based on two basic assumptions: (i) the $3z^2-r^2$ and x^2-y^2 orbitals are degenerate, and (ii) the energy of the system depends, essentially, on superexchange interactions between these orbitals. In 1973, they applied the orbital model to K_2CuF_4 predicting an antiferrodistortive orbital order at the *I4/mmm* phase, characterized by electrons in alternating $3x^2-r^2/3y^2-r^2$ orbitals, which would be the seed that leads to the orthorhombic distortion.[81] Moreover, they argued that this orbital antiferrodistortive order was necessary to obtain an FM ordering. However, the results in the previous section clearly show that the assumptions of the orbital ordering model are not correct. There exists a large gap between the a_{1g} and b_{1g} states in the *I4/mmm* parent phase, so the orbitals are not degenerate favoring the hole to move to the $3z^2-r^2$ orbital in fluoride lattices. This FM ordering of the orbitals would be contrary to that predicted by the Kugel−Khomskii model and would lead to AFM ordering in the *I4/mmm* parent phase. This will be confirmed by first-principles simulations below. Moreover, if the orbital ordering is applicable to K_2CuF_4, then it would also be applicable to La_2CuO_4, a system well known for its strong AFM ordering.[11] Thus, we believe that the use of the orbital ordering model in these lattices is compromised,[6] and the origin of the magnetic structure should be reanalyzed in detail.

When in the M_A-F-M_B exchange path (Figure 2), the involved angle, $\phi(M_A-F-M_B)$, is equal to 180° it usually gives rise to an AFM ordering, a situation found in the tetragonal K_2NiF_4 and K_2NiF_4 compounds belonging to the *I4/mmm* space group as well as in the cubic perovskite $KNiF_3$.[38] For this reason, the experimental FM arrangement displayed in the layer planes of both Cs_2AgF_4 and K_2CuF_4 compounds with a *Cmca* crystal structure and $\phi(M_A-F-M_B)$ = 180° is puzzling. Furthermore, there are also huge differences in the transition temperature, T_c. Indeed, K_2NiF_4 is AFM up to a temperature T_c = 97.23 K,[38] while for K_2CuF_4 and Cs_2AgF_4, the FM order disappears at much lower temperatures, namely, at T_c = 6.5[7] and 15 K,[28] respectively. This situation is, in principle, surprising as, in superexchange interactions, an increase in the covalency tends to enhance T_c as it happens on passing from $RbMnF_3$ (T_c = 83 K) to $KNiF_3$ (246 K).[38] However, the

https://doi.org/10.1021/acs.jpcc.3c03895
J. Phys. Chem. C 2023, 127, 16695−16708

Table 4. Comparison of Experimental Data for the Layered Compound K_2NiF_4[38a]

compound	phase	data	R_z (Å)	$R_x = R_y$ (Å)	ΔE (meV)	J (meV)
K_2NiF_4	$I4/mmm$	experimental	2.001	2.006	53.1	8.9
K_2CuF_4	$I4/mmm$	calculated	1.906	2.061	4.4	2.2
Cs_2AgF_4	$I4/mmm$	calculated	2.081	2.292	7.92	3.9

[a]The Ni^{2+} spin is $S = 1$, with those calculated in this work for K_2CuF_4 and Cs_2AgF_4 in the parent $I4/mmm$ phase. The spin of d^9 ions is $S = {}^1/_2$. $\Delta E = E(\mathrm{FM}) - E(\mathrm{AFM})$ per magnetic ion and depends on the exchange constant, J, and the spin of the magnetic cation.

optical electronegativity[19] for Ni^{2+} ($\chi = 2.2$) is smaller than that for Cu^{2+} ($\chi = 2.4$) or Ag^{2+} ($\chi = 2.8$)[18,76] and then, in a simple view, one would expect a smaller covalency and T_c value for K_2NiF_4 than for compounds involving d^9 cations.

Seeking to clear these puzzling issues up, we follow the procedure employed in Section 3.2, thus exploring in a first step the behavior of K_2CuF_4 and Cs_2AgF_4 in the $I4/mmm$ parent phase. To achieve this goal, we have calculated the total energy per magnetic ion, $E(\mathrm{FM})$ and $E(\mathrm{AFM})$, corresponding, respectively, to the FM and AFM phases associated with the same crystal structure, and from them, we derive the key quantity $\Delta E = E(\mathrm{FM}) - E(\mathrm{AFM})$. It should first be stressed that the equilibrium geometry obtained for both magnetic configurations is essentially the same as they involve differences in metal−ligand distances smaller than 5×10^{-3} Å. The obtained ΔE values for both K_2CuF_4 and Cs_2AgF_4 are displayed in Table 4 and lie in the range of 1−10 meV, and thus, they are much smaller than $|E(\mathrm{AFM})|$. For instance, for K_2CuF_4, $\Delta E/|E(\mathrm{AFM})| \approx 5 \times 10^{-8}$, a fact that once more underlines the subtle origin of magnetic ordering.

The value $\Delta E = 53.1$ meV for K_2NiF_4 in Table 4 is derived from the experimental exchange constant, $J = 8.85$ meV, associated with two coupled cations (eq 1) using the expression

$$\Delta E = zJS_{\max}(S_{\max} + 1)/4 \tag{15}$$

Here, z means the number of neighbor cations, equal to 4 for a layered compound, while $S_{\max}$ is the maximum value of the total spin corresponding to two coupled cations with spin S, thus equaling to 2 for K_2NiF_4.

The main source of ΔE in compounds like $KNiF_3$ or K_2NiF_4 has been explained by Anderson and Hay et al. just considering a simple M −F−M symmetric dimer.[77,79] According to these models, ΔE is essentially related to valence electrons and involves the difference of two contributions

$$\Delta E = E_V(\mathrm{FM}) - E_V(\mathrm{AFM}) \tag{16}$$

where the $E_V(\mathrm{FM})$ and $E_V(\mathrm{AFM})$ contributions associated only with valence electrons are both negative and favor the FM and AFM configuration, respectively. These contributions typically lie in the range of 1−100 meV. In the same vein, the exchange constant, J, of two coupled cations (eqs 1 and 15) can be expressed as the difference between two positive contributions

$$J = J(\mathrm{AFM}) - J(\mathrm{FM}) \tag{17}$$

According to the work by Anderson et al. on a symmetric dimer, the $J(\mathrm{AFM})$ contribution greatly depends on the charge transferred from the cation to the ligand in orbitals containing unpaired electrons.[77−79] For clarifying this issue, we start considering a NiF_6^{4-} unit in the cubic $KNiF_3$ compound that involves two unpaired electrons in the $|\theta\rangle$ and $|\varepsilon\rangle$ antibonding molecular orbitals (Figure 6), described by[82]

$$|\theta\rangle = N\{|d(3z^2 - r^2)\rangle - (\mu/\sqrt{12})[2(|p_\sigma(5)\rangle + |p_\sigma(6)\rangle) - (|p_\sigma(1)\rangle + |p_\sigma(2)\rangle + |p_\sigma(3)\rangle + |p_\sigma(4)\rangle)]\}$$

$$|\varepsilon\rangle = N\{|d(x^2 - y^2)\rangle - (\mu/2)[|p_\sigma(1)\rangle - |p_\sigma(2)\rangle + |p_\sigma(3)\rangle - |p_\sigma(4)\rangle]\} \tag{18}$$

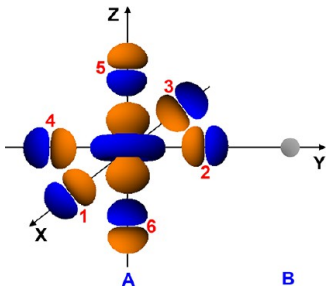

Figure 6. Picture of the antibonding $|\theta\rangle \sim 3z^2-r^2$ molecular orbital for an octahedral NiF_6^{4-} unit in cubic $KNiF_3$ perovskite.

Due to the existence of covalency, the two non-filled orbitals of a simple NiF_6^{4-} unit do not have pure $|d(3z^2-r^2)\rangle$ or $|d(x^2-y^2)\rangle$ characters, thus involving a partial transfer of charge from metal to six ligands. If we consider the bridging ligand number 2 (Figure 6), then the charges transferred to it in σ-orbitals $|\theta\rangle$ and $|\varepsilon\rangle$ are equal to $(N\mu)^2/12$ and $(N\mu)^2/4$, respectively, thus implying a total charge, termed f_σ, equal to

$$f_\sigma(NiF_6^{4-}) = (N\mu)^2/3 \tag{19}$$

Due to cubic symmetry in $KNiF_3$, the same charge is transferred to any ligand of the NiF_6^{4-} unit. Obviously, if we consider a M_A− F(2)−M_B dimer (Figure 6), then the charge transferred from M_A to the bridging ligand, $f_\sigma(A)$, is the same as that from M_B, $f_\sigma(B)$, provided that the dimer is symmetric and then we can write $f_\sigma(A) = f_\sigma(B) = f_\sigma$. This symmetric situation happens in both $KNiF_3$ and K_2NiF_4, although in the last case, only the four ligands[38] of a NiF_6^{4-} unit in the layer plane are involved in the superexchange.

A central issue in the work by Anderson et al. on a symmetric dimer is the dependence of the $J(\mathrm{AFM})$ contribution on f_σ that, for the present purposes, can simply be written as[77−79]

$$J(\mathrm{AFM}) \propto f_\sigma^{\,2} \tag{20}$$

This fact agrees with the measured decrease[38] in J on passing from $KNiF_3$ (8.4 meV) to $RbMnF_3$ (0.57 meV) following the smaller covalency[78,82−85] in MnF_6^{4-} ($f_\sigma \sim 1\%$) than in NiF_6^{4-} ($f_\sigma \sim 4\%$), a result also consistent with the lower optical electronegativity of Mn^{2+} ($\chi \approx 1.4$)[19,22,86,87] when compared[19] to $\chi = 2.2$ for Ni^{2+}.

https://doi.org/10.1021/acs.jpcc.3c03895
J. Phys. Chem. C 2023, 127, 16695−16708

The NiF_6^{4-} complex in the tetragonal K_2NiF_4 compound is nearly octahedral (Table 4), with metal−ligand distances $R_x = R_y = 2.006$ Å and $R_z = 2.001$ Å, which are very close to $R = 2.007$ Å measured[38] in the cubic perovskite $KNiF_3$. As the Ni^{2+} spin in the electronic ground state of K_2NiF_4 is also $S = 1$, the exchange constant J in K_2NiF_4 (8.9 meV) and $KNiF_3$ (8.7 meV) derived from experimental data are very near. Despite this fact, the transition temperature T_c is higher for $KNiF_3$ (246 K) than for the layered compound K_2NiF_4 (97.2 K) as a result of the different numbers of neighbor cations, z, in both compounds.[88]

It is worth noting now that, if we move from K_2NiF_4 to K_2CuF_4, keeping the *I4/mmm* structure, then the number of unpaired electrons is reduced from 2 to 1. Furthermore, the unpaired electron in K_2CuF_4 is located in a $|3z^2-r^2\rangle$ molecular orbital of a D_{4h} CuF_6^{4-} complex helped by the electrostatic potential, $V_R(\mathbf{r})$, due to the rest of the lattice ions (Figure 2). It should be noticed that in this orbital, coming from $|\theta\rangle$ in O_h symmetry, the dominant bonding is with the two axial ligands, while the charge transferred to the in-plane bridging ligands is smaller. More precisely, if, as a rough first step, we approximate $|3z^2-r^2\rangle$ by $|\theta\rangle$, then we obtain for the bridge ligand $f_\sigma(CuF_6^{4-}) = (N\mu)^2/12$, which is thus 4 times smaller than the value $f_\sigma = (N\mu)^2/3$ derived for (NiF_6^{4}) (eq 19), provided that $N\mu$ is the same for both systems.

Seeking to clarify this central issue, we have calculated the f_σ value for both the bridging and axial ligands of K_2CuF_4 and Cs_2AgF_4 in the *I4/mmm* parent phase. Results are collected in Table 5 and compared to those for K_2NiF_4. They confirm that

Table 5. Calculated Charge Transferred to Axial and Equatorial Ligands for the Hole of MF_6^{4-} Units (M = Cu and Ag) in K_2CuF_4 and Cs_2AgF_4 Compounds in the *I4/mmm* Parent Phase[a]

compound	phase	f_σ(axial) (%)	f_σ(bridging) (%)	ΔE (meV)
K_2CuF_4	*I4/mmm*	7.98	1.70	4.4
Cs_2AgF_4	*I4/mmm*	11.28	2.43	7.92
K_2NiF_4	*I4/mmm*	4.1	4.1	53.1

[a]Results are compared to those for K_2NiF_4 with two unpaired electrons. The ΔE values calculated for the three systems are also included for comparison.

f_σ is much higher for axial than for the in-plane bridging ligands of K_2CuF_4 and Cs_2AgF_4, thus stressing that covalency in the latter ligands is residual. At the same time, they show that AgF_6^{4-} is more covalent than CuF_6^{4-} in accord with the electronegativity scale. Despite these facts, the f_σ values derived for bridging ligands in K_2CuF_4 (1.70%) and Cs_2AgF_4 (2.43%) are clearly smaller than $f_\sigma = 4.1\%$ calculated for K_2NiF_4 and $KNiF_3$. Values of f_σ in the range of 3.5−6% have been reported for NiF_6^{4-} by other authors.[78,82−85] This relevant fact is thus consistent with the smaller J value derived for K_2CuF_4 and Cs_2AgF_4 when compared to that for K_2NiF_4 (Table 4). Now, if we take into account the different value of $S_{max}(S_{max}+1)$ in both compounds, then this explains why ΔE is 1 order of magnitude higher in the case of K_2NiF_4.

A key question in the present analysis is to understand the influence of the *I4/mmm* → *Cmca* structural transition upon the magnetic ordering[6] of K_2CuF_4 and Cs_2AgF_4. In that process, the MF_6^{4-} complexes (M = Cu and Ag) change from tetragonal to orthorhombic symmetry, a distortion described by the Q coordinate (Figure 4).

The variation of $\Delta E = E(FM) - E(AFM)$ calculated for Cs_2AgF_4 as a function of the Q distortion coordinate is displayed in Figure 7. For simplicity, in that figure, E(FM) is

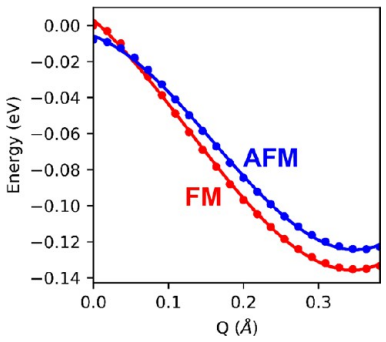

Figure 7. Energy (given per formula unit) of Cs_2AgF_4 obtained by single-point calculations throughout the antiferrodistortive distortion from the parent tetragonal *I4/mmm* phase to the minimum at the orthorhombic *Cmca* one. These data are similar to those reported in ref 6, although in that article, the abscissa reflects the position of the bridge ligand and not the distortion coordinate, Q.

chosen to be equal to zero for $Q = 0$. As a salient feature, Figure 7 shows that a small orthorhombic distortion induces a change of sign of ΔE, and thus, Cs_2AgF_4 becomes FM at the final equilibrium geometry ($Q = 0.34$ Å). A similar situation is found[6] for K_2CuF_4. Experimental and calculated ΔE and J values at the equilibrium structures of Cs_2AgF_4 and K_2CuF_4 are collected in Table 6.

Table 6. Experimental and Calculated ΔE and J Values (in meV) at the Equilibrium Structures of Cs_2AgF_4 and K_2CuF_4 Described in Tables 1 and 2[a]

compound	phase	ΔE(exper)	J(exper)	ΔE(calc)	J(calc)
Cs_2AgF_4	*Cmca*	−7.58	−3.79	−11.2	−5.6
K_2CuF_4	*Cmca*	−3.44	−1.72	−5.3	−2.7

[a]Experimental data come from ref 28 for Cs_2AgF_4 and ref 7 for K_2CuF_4.

It is worthwhile to remark that, on passing from $Q = 0$ to the equilibrium geometry in Figure 7, there is an energy gain of around 140 meV per formula unit driven by the vibronic interaction of eq 8. When this quantity is compared to $\Delta E = 7.92$ meV at $Q = 0$ (Table 4), we then realize that the magnetism in Cs_2AgF_4 is just a consequence of vibronic coupling in the electronic ground state.

The switch to an FM arrangement induced by the orthorhombic distortion in Cs_2AgF_4 can be understood through the ideas by Anderson et al.[77,78] on a M_A-F-M_B dimer, which in that situation is no longer symmetric. If we consider the complex associated with the cation at A (Figure 2), then the charge transferred to ligands placed at the local x axis is expected to be higher than that corresponding to ligands placed along the local y axis that involve a higher metal−ligand distance as a result of the orthorhombic distortion. Accordingly, we can write

$$f_\sigma(A, x) > f_\sigma(A, y)$$

$$f_\sigma(B, x) = f_\sigma(A, x) > f_\sigma(B, y) = f_\sigma(A, y) \quad (21)$$

https://doi.org/10.1021/acs.jpcc.3c03895
J. Phys. Chem. C 2023, 127, 16695−16708

Table 7. Charge Transferred to Ligands in the Layer Plane for the *Cmca* Equilibrium Geometry of K_2CuF_4 and Cs_2AgF_4[a]

system	complex	symmetry	R_x	R_y	$f_\sigma(x)$ (%)	$f_\sigma(y)$ (%)
K_2CuF_4	CuF_6^{4-}	tetragonal	2.061	2.061	1.70	1.70
		orthorhombic	1.941	2.234	4.86	0
Cs_2AgF_4	AgF_6^{4-}	tetragonal	2.292	2.292	2.43	2.43
		orthorhombic	2.106	2.458	6.82	0
$NH_4Cl:Cu^{2+}$ (pH = 7)	$CuCl_4(NH_3)_2^{2-}$	tetragonal	2.78	2.78	4.70	4.70
$NH_4Cl:Cu^{2+}$(pH = 3)	$CuCl_4(H_2O)_2^{2-}$	orthorhombic	2.52	2.97	8.7	0

[a]In this table, $f_\sigma(x) \equiv f_\sigma(A,x)$ and $f_\sigma(y) \equiv f_\sigma(A,y)$ correspond to close and far ligands of a given complex lying along x and y directions, respectively. For the sake of completeness, the value $f_\sigma(x) = f_\sigma(y)$ associated with the tetragonal parent phase is also collected. The results are compared to those derived from EPR experiments on $CuCl_4(NH_3)_2^{2-}$ and $CuCl_4(H_2O)_2^{2-}$ centers formed in $NH_4Cl:Cu^{2+}$ crystals grown in solution with different pH. While the equilibrium geometry of $CuCl_4(NH_3)_2^{2-}$ is tetragonal with the four Cl^- ions, lying in a plane perpendicular to the main axis, at the same distance from Cu^{2+} in $CuCl_4(H_2O)_2^{2-}$, there is an orthorhombic distortion in the plane formed by chlorine ions. The values of R_x and R_y distances (in Å) for these centers are taken from ref 70.

A central issue in the analysis of a non-symmetric dimer is the dependence of the J(AFM) contribution upon the quantities $f_\sigma(A,x)$ and $f_\sigma(B,y)$ involved in the bridging ligand of Figure 2. Following a similar procedure to that by Anderson in the symmetric dimer,[77] this can easily be obtained[6]

$$J(\mathrm{AFM}) \propto f_\sigma(\mathrm{A},x)\, f_\sigma(\mathrm{B},y) = f_\sigma(\mathrm{A},x)\, f_\sigma(\mathrm{A},y) \qquad (22)$$

This result just means that, if bonding is significantly reduced in the longer F−M_B bond, then the exchange constant, J, could then be dominated by the FM contribution, J(FM), which is less sensitive to chemical bonding than J(AFM). Indeed, the dependence of J(FM) on $f_\sigma(A,x)$ and $f_\sigma(A,y)$ has the form[6] $p_x f_\sigma(A,x) + p_y f_\sigma(A,y)$, thus implying that J(FM) is not zero even if $f_\sigma(A,y) = 0$.

According to eq 22, it is therefore crucial to determine the charge transferred to the ligand in the short, $f_\sigma(A,x)$, and long, $f_\sigma(A,y)$, bonds in the equilibrium geometry of both Cs_2AgF_4 and K_2CuF_4 compounds. Henceforth, these charges are simply denoted as $f_\sigma(x)$ and $f_\sigma(y)$, respectively.

Results of present calculations on this central issue are portrayed in Table 7. As a salient feature, the obtained value of $f_\sigma(y)$ is equal to zero at the *Cmca* equilibrium geometry of both Cs_2AgF_4 and K_2CuF_4 compounds, a fact that strongly suggests that the AFM contribution, J(AFM), disappears. In other words, this key fact means that the orthorhombic distortion unveils the J(FM) contribution to J that is somewhat hidden in the *I*4/*mmm* parent phase. According to this view and the calculated values in Tables 4 and 5, we can estimate that J(AFM) ≈ 9.6 meV and J(FM) ≈ 5.6 meV for the *I*4/*mmm* parent phase of Cs_2AgF_4, while J(AFM) ≈ 4.9 meV and J(FM) ≈ 2.7 meV would correspond to K_2CuF_4.

It is worthwhile to remark that the present results are underpinned by EPR data carried out on $CuCl_4X_2^{2-}$ centers (X = NH_3 and H_2O) formed in $NH_4Cl:Cu^{2+}$ crystals grown in solutions with different pH.[89,90,75] While the equilibrium geometry of $CuCl_4(NH_3)_2^{2-}$ is tetragonal with four equivalent Cl^- ions, lying in a plane perpendicular to the main axis, in $CuCl_4(H_2O)_2^{2-}$, there is an orthorhombic distortion in the plane formed by chlorine ions.[70,75] Interestingly, no superhyperfine interaction of the unpaired electron with the two far chlorine nuclei of the $CuCl_4(H_2O)_2^{2-}$ center has been observed by EPR,[75] thus proving that $f_\sigma(y) = 0$. Moreover, from EPR data, the calculated charge transferred to one of the close Cl nuclei in $CuCl_4(H_2O)_2^{2-}$ ($f_\sigma(x)$ = 8.7%) is about twice that found for the tetragonal $CuCl_4(NH_3)_2^{2-}$ species, as it is also shown on Table 7.

The present results thus prove that the FM displayed in the layer planes of Cs_2AgF_4 and K_2CuF_4 is strongly dependent on the orthorhombic distortion.[6] As discussed in Section 3.2, that distortion is fostered by the allowed vibronic coupling of the $^2A_{1g}$ ground state of a tetragonal MF_6^{4-} complex (M = Cu and Ag) with the excited $^2B_{1g}$ state through the local b_{1g} distortion mode.

It is worth noting now that a similar situation cannot take place for K_2NiF_4 where the ground state of the tetragonal NiF_6^{4-} complex is $^3B_{1g}$ simply described[82] by the Slater determinant $|x^2-y^2\uparrow\ 3z^2-r^2\uparrow|$. Indeed, the $^1A_{1g}$ excited state $|3z^2-r^2\uparrow\ 3z^2-r^2\downarrow|$ cannot vibronically be coupled to the $^3B_{1g}$ ground state as the spin in both states is different, a matter already discussed in Section 3.2. Furthermore, a $^3B_{1g}$ ground state can only vibronically be coupled to $^3A_{1g}$ excited states if a b_{1g} distortion mode is involved. However, within the 45 states emerging from the d^8 configuration, there are no $^3A_{1g}$ states in a local D_{4h} symmetry.[82] This simple reasoning thus sheds some light on the lack of orthorhombic distortion in K_2NiF_4 and thus its AFM behavior. Along this line, the ground state of the MnF_6^{4-} complex in the *I*4/*mmm* K_2MnF_4 crystal has a spin S = 5/2. Accordingly, it cannot be coupled vibronically to any of the rest of the 246 states coming from the d^5 configuration,[82] which have at most S = 3/2. This relevant fact also helps to avoid the orthorhombic instability in K_2MnF_4. According to this reason, the local $O_h \rightarrow T_d$ symmetry change observed[91] for $BaF_2:Mn^{2+}$ involves the coupling of the electronic ground state (S = 5/2) with a charge transfer state of the same spin.[92]

3.6. Insight into Rb_2AgF_4. The Rb_2AgF_4 compound was also first synthesized by Odenthal et al.[25] in 1974 and subsequently explored by Friebel and Reinen[43] through EPR and optical spectroscopy. Despite the fact that the structure of Rb_2AgF_4 was not determined, the closeness of their experimental EPR and optical data to those reported for Cs_2AgF_4 already suggested that both compounds could display the same crystal structure. In 2016, Kurzydłowski et al. carried out DFT + U calculations on the Rb_2AgF_4 compound.[93] Although these authors find that the stable phase of Rb_2AgF_4 is described by the *Cmca* space group, they do not report the values of lattice parameters nor Ag^{2+}−F^- distances.

For this reason, we have carried out DFT calculations, with the PW1PW hybrid functional, seeking to optimize the geometry of Rb_2AgF_4 in three possible layered phases, namely, *Cmca*, *I*4/*mmm*, and $P2_1/c$. The $P2_1/c$ structure is included as it seems to be involved[92] in K_2AgF_4 and Na_2AgF_4. Of course, for each kind of structure, we have also explored both the FM and AFM arrangements of magnetic moments arising from

https://doi.org/10.1021/acs.jpcc.3c03895
J. Phys. Chem. C 2023, 127, 16695−16708

Table 8. Calculated Lattice Parameters (Axes a, b, and c, in Å, and Monoclinic Angle β, in Degrees) and Metal−Ligand Distances (Axial R_z and Equatorials R_x and R_y, All in Å) for Rb_2AgF_4 in Three Different Structures (Orthorhombic *Cmca*, Tetragonal *I4/mmm*, and Monoclinic $P2_1/c$) and Two Magnetic Orders (FM and AFM)[a]

		a	b	c	β	R_z	R_x	R_y	E_r
Cmca	FM	13.509	6.373	6.372	90	2.109	2.076	2.430	0
	AFM	13.502	6.379	6.379	90	2.109	2.074	2.437	+12
I4/mmm	FM	4.521	4.521	13.360	90	2.066	2.261	2.261	+150
	AFM	4.522	4.522	13.350	90	2.063	2.261	2.261	+133
$P2_1/c$	FM	3.885	10.627	6.713	91.0	2.076	2.092	2.909	+130
	AFM	3.885	10.628	6.714	91.0	2.076	2.092	2.910	+130

[a] E_r is the difference in energy (in meV/formula) with respect to the phase with minimum energy (FM *Cmca*). Note the different notations of the long axis in each structure.

silver ions. Results are gathered in Table 8 where the relative energy, E_r, of six considered phases is reported, and $E_r = 0$ corresponds to the *Cmca* structure with FM ordering.

The calculated E_r values in Table 8 mean that the stable phase in Rb_2AgF_4 corresponds to a *Cmca* structure with FM ordering such as it is experimentally found for Cs_2AgF_4. Moreover, if we consider for Rb_2AgF_4 an AFM ordering, keeping the *Cmca* structure, then the changes of $Ag^{2+}-F^-$ distances are smaller than 0.01 Å and $E_r = 12$ meV. In this case, E_r is equal to the quantity $-\Delta E$ used in Section 3.5. Thus, the value $E_r = -\Delta E = 12$ meV found for Rb_2AgF_4 is similar to that for Cs_2AgF_4 reflected in the results of Table 6 and Figure 7 of Section 3.5. Along this line, the values of $Ag^{2+}-F^-$ distances calculated for Rb_2AgF_4 in the stable phase (Table 8) are certainly close to $R_z = 2.112$ Å, $R_x = 2.111$ Å, and $R_y = 2.441$ Å obtained for Cs_2AgF_4 (Table 1). This result is thus consistent with the practically identical d−d transitions[43] and EPR spectra[26,43] measured experimentally for both Rb_2AgF_4 and Cs_2AgF_4. For instance, the accurate EPR measurements carried out by Kurzydłowski et al. give[26] $g(\mathbf{a}) = 2.076$ and $g(\perp\mathbf{a}) = 2.26$ for Rb_2AgF_4 and $g(\mathbf{a}) = 2.077$ and $g(\perp\mathbf{a}) = 2.257$ for Cs_2AgF_4.

Concerning the *I4/mmm* parent phase with AFM ordering, the present results on Rb_2AgF_4 yield $E_r = 133$ meV, a quantity nearly identical to that derived for Cs_2AgF_4, as shown in Figure 7 (Section 3.5). According to the results of Table 8, such a parent phase should be unstable. We have verified that in that situation, there are two modes, b_{1g} and a_{2g}, with the same imaginary frequency of 401i cm^{-1}, which correspond to similar orthorhombic distortions of the F ligands within a plane but for the $z = 0$ and 1/2 layers, respectively.

Regarding a possible monoclinic $P2_1/c$ structure, the results of Table 8 imply an energy per magnetic ion, which is again 130 meV above that for the stable phase of Rb_2AgF_4.

4. FINAL REMARKS

The present results stress the importance of exploring the *I4/mmm* parent phase of K_2CuF_4 and Cs_2AgF_4 for understanding the origin of their magnetic properties, very distinct from those exhibited by other layered fluorides like K_2NiF_4 or K_2MnF_4. At the same time, they prove that the ferromagnetism observed for both K_2CuF_4 and Cs_2AgF_4 compounds greatly depends on the orthorhombic distortion.[94] As explained in Sections 3.2 and 3.5, that instability is driven by the allowed vibronic admixture of the $^2A_{1g}$ ground state of a tetragonal MF_6^{4-} complex (M = Cu and Ag) with the excited $^2B_{1g}$ state. On the contrary, the lack of excited states, which, within the d^5 configuration, can be vibronically coupled with the ground state, hampers the orthorhombic distortion in K_2MnF_4. This situation is thus similar to that taking place in $SrCl_2$ where the d^9 impurities Ni^+, Cu^{2+}, and Ag^{2+} all move off-center,[21,22,95] while a Mn^{2+} impurity remains[96] at the Sr^{2+} site. Nevertheless, for d^9 impurities, this situation changes when we replace $SrCl_2$ by CaF_2 where only Ni^+ moves off-center while Ag^{2+} and Cu^{2+} remain at the Ca^{2+} site.[22] The substitution of chlorine by fluorine, the increase in the nominal charge of the cation, and the reduction of interatomic distances all tend to increase the value of the K_0 contribution in eq 9, and thus, they help to suppress the off-center instability.

These ideas also shed light on the occurrence of ferroelectricity in $BaTiO_3$ but not in $CaTiO_3$ involving smaller interatomic distances. Indeed, an isolated Ti^{4+} cannot move spontaneously off-center in these perovskites, but at equilibrium, K_0 is higher for $CaTiO_3$ than for $BaTiO_3$ following the smaller interatomic distances. As ferroelectricity requires the simultaneous off-center motion of all Ti^{4+} ions, this explains,[97] albeit qualitatively, why $BaTiO_3$ is better suited than $CaTiO_3$.

In the case of Cu^{2+} complexes, the existence of close excited states that can vibronically be mixed with the ground state favors changes of the electronic density and the associated distortion, provided that $K < 0$. This characteristic of Cu^{2+} complexes not shared by the high spin Mn^{2+} or Ni^{2+} ones is sometimes referred to as plasticity.[98]

From the present analysis, an understanding of optical and magnetic properties of layered compounds with d^9 ions requires to explore the influence of the electrostatic potential, $V_R(\mathbf{r})$, in the parent phase and the possible instabilities driven by a force constant that becomes negative. By contrast, the attempts to explain such properties assuming a JT effect in tetragonal, orthorhombic, or monoclinic lattices are meaningless. An exception to this behavior is the widely studied AgF_2[99] whose parent phase is cubic. In this case, the AgF_6^{4-} units are trigonally distorted, and thus, under this symmetry, the ground state is strictly degenerate, making possible the existence of a JT effect as it has recently been discussed.[50]

Further work on silver fluorides like K_2AgF_4[100] or Na_2AgF_4 is now underway.

AUTHOR INFORMATION

Corresponding Author

José Antonio Aramburu − *Departamento de Ciencias de la Tierra y Física de la Materia Condensada, Universidad de Cantabria, 39005 Santander, Spain;* orcid.org/0000-0002-5030-725X; Email: antonio.aramburu@unican.es

https://doi.org/10.1021/acs.jpcc.3c03895
J. Phys. Chem. C 2023, 127, 16695−16708

Authors

Inés Sánchez-Movellán − *Departamento de Ciencias de la Tierra y Física de la Materia Condensada, Universidad de Cantabria, 39005 Santander, Spain*

Guillermo Santamaría-Fernández − *Departamento de Ciencias de la Tierra y Física de la Materia Condensada, Universidad de Cantabria, 39005 Santander, Spain*

Pablo García-Fernández − *Departamento de Ciencias de la Tierra y Física de la Materia Condensada, Universidad de Cantabria, 39005 Santander, Spain*

Miguel Moreno − *Departamento de Ciencias de la Tierra y Física de la Materia Condensada, Universidad de Cantabria, 39005 Santander, Spain*

Complete contact information is available at: https://pubs.acs.org/10.1021/acs.jpcc.3c03895

Notes

The authors declare no competing financial interest.

■ ACKNOWLEDGMENTS

We acknowledge the financial support from grant no. PGC2018-096955-B-C41 funded by MCIN/AEI/10.13039/501100011033. I.S.-M. (grant BDNS:589170) and G.S.-F. acknowledge the financial support from Universidad de Cantabria and Gobierno de Cantabria.

■ REFERENCES

(1) Correa-Baena, J. P.; Saliba, M.; Buonassisi, T.; Grätzel, M.; Abate, A.; Tress, W.; Hagfeldt, A. Promises and challenges of perovskite solar cells. *Science* **2017**, *358*, 739−744.

(2) Akkerman, Q. A.; Manna, L. What defines a halide perovskite? *ACS Energy Lett.* **2020**, *5*, 604−610.

(3) Jaffe, A.; Lin, Y.; Mao, W. L.; Karunadasa, H. I. Pressure-induced conductivity and yellow-to-black piezochromism in a layered Cu−Cl hybrid perovskite. *J. Am. Chem. Soc.* **2015**, *137*, 1673−1678.

(4) Gupta, S.; Pandey, T.; Singh, A. K. Suppression of Jahn−Teller distortions and origin of piezochromism and thermochromism in Cu−Cl hybrid perovskite. *Inorg. Chem.* **2016**, *55*, 6817−6824.

(5) Carrasco-Busturia, D.; Sánchez-Movellán, I.; Tygesen, A. S.; Bhowmik, A.; García-Lastra, J. M.; Aramburu, J. A.; Moreno, M. Red shift in optical excitations on layered copper perovskites under pressure: role of the orthorhombic instability. *Chem. − Eur. J.* **2023**, *29*, No. e202202933.

(6) Sánchez-Movellán, I.; Moreno, M.; Aramburu, J. A.; García-Fernández, P. Strain-induced ferromagnetic to antiferromagnetic crossover in d^9-Ion (Cu^{2+} and Ag^{2+})-layered perovskites. *J. Phys. Chem. C* **2023**, *127*, 8332−8341.

(7) Yamada, I. Magnetic Properties of K_2CuF_4: A transparent two-dimensional ferromagnet. *J. Phys. Soc. Jpn.* **1972**, *33*, 979−988.

(8) Hidaka, M.; Inoue, K.; Yamada, I.; Walker, P. J. X-ray diffraction study of the crystal structures of K_2CuF_4 and $K_2Cu_xZn_{1-x}F_4$. *Physica B +C* **1983**, *121*, 343−350.

(9) Ishizuka, M.; Terai, M.; Hidaka, M.; Endo, S.; Yamada, I.; Shimomura, O. Pressure-induced structural phase transition in the two-dimensional Heisenberg ferromagnet K_2CuF_4. *Phys. Rev. B: Condens. Matter Mater. Phys.* **1998**, *57*, 64−67.

(10) Riley, M. J.; Dubicki, L.; Moran, G.; Krausz, E. R.; Yamada, I. Optical spectrum of K_2CuF_4. *Inorg. Chem.* **1990**, *29*, 1614−1626.

(11) García-Fernández, P.; Moreno, M.; Aramburu, J. A. Electrostatic control of orbital ordering in noncubic crystals. *J. Phys. Chem. C* **2014**, *118*, 7554−7561.

(12) Aramburu, J. A.; García-Fernández, P.; Mathiesen, N. R.; García-Lastra, J. M.; Moreno, M. Changing the usual interpretation of the structure and ground state of Cu^{2+}-layered perovskites. *J. Phys. Chem. C* **2018**, *122*, 5071−5082.

(13) Steadman, J. P.; Willett, R. D. The crystal structure of $(C_2H_5NH_3)_2CuCl_4$. *Inorg. Theor. Chim. Acta* **1970**, *4*, 367−371.

(14) Ohwada, K.; Ishii, K.; Inami, T.; Murakami, Y.; Shobu, T.; Ohsumi, H.; Ikeda, N.; Ohishi, Y. Structural properties and phase transition of holt-orbital-ordered $(C_2H_5NH_3)_2CuCl_4$ studied by resonant and non-resonant x-ray scatterings under high pressure. *Phys. Rev. B* **2005**, *72*, No. 014123.

(15) Lim, A. R.; Kwac, L. K. Advances in physicochemical characterization of lead-free hybrid perovskite $[NH_3(CH_2)_3NH_3]$-$CuBr_4$ crystals. *Sci. Rep.* **2022**, *12*, 8769.

(16) Choi, M. Y.; Lee, S. J.; Ju, H.; Lim, A. R. Phase transition, thermal stability, and molecular dynamics of organic−inorganic hybrid perovskite $[NH_3(CH_2)_6NH_3]CuCl_4$ crystals. *RSC Adv.* **2022**, *12*, 20679−20685.

(17) Grochala, W. Silverland: the realm of compounds of divalent silver − and why they are interesting. *J. Supercond. Novel Magn.* **2018**, *31*, 737−752.

(18) Aramburu, J. A.; Moreno, M. The anomalous quasi isotropic (g) tensor found for $CdBr_2$:Ag^{2+} and $AgBr_{0.15}Cl_{0.85}$:Ag^{2+}: An explanation through strong covalency. *Solid State Commun.* **1987**, *62*, 513−516.

(19) Jørgensen, C. K. Electron transfer spectra. In *Prog. Inorg. Chem.*; S. J., Lippard, Eds.; John Wiley & Sons, Inc.: New York, 1970; pp. 101−158.

(20) Sierro, J. Paramagnetic resonance of the Ag^{2+} ion in irradiated alkali chlorides. *J. Phys. Chem. Solids* **1967**, *28*, 417−422.

(21) Bill, H. *Observation of the Jahn-Teller Effect with Electron Paramagnetic Resonance in The Dynamical Jahn-Teller Effect in Localized Systems*; Perlin, Y. E., Wagner, M., Eds.; Elsevier: Amsterdam, 1984; pp. 754.

(22) Moreno, M.; Barriuso, M. T.; Aramburu, J. A.; García-Fernández, P.; García-Lastra, J. M. Microscopic insight into properties and electronic instabilities of impurities in cubic and lower symmetry insulators: the influence of pressure. *J. Phys.: Condens. Matter* **2006**, *18*, R315−R360.

(23) Miyanaga, T. EPR studies of strong Jahn-Teller coupling systems $CdCl_2$:Ag^{2+} and $CdBr_2$:Ag^{2+}. *J. Phys. Soc. Jpn.* **1979**, *46*, 167−175.

(24) Yamaga, M.; Hayahsi, Y.; Yoshioka, H. Jahn-Teller Effect in the ESR spectrum of $(AgBr_6)^{4-}$ in Mixed Crystals $AgBr_{1-x}Cl_x$. *J. Phys. Soc. Jpn.* **1979**, *47*, 677−678.

(25) Odenthal, R.-H.; Paus, D.; Hoppe, R. Zur magnetochemie des zweiwertigen silbers neue fluoroargentate(II): Cs_2AgF_4, Rb_2AgF_4, und K_2AgF_4. *Z. anorg. allg. Chem.* **1974**, *407*, 144−150.

(26) Kurzydłowski, D.; Jaroń, T.; Ozarowski, A.; Hill, S.; Jaglicić, Z.; Filinchuk, Y.; Mazej, Z.; Grochala, W. Local and cooperative Jahn−Teller Effect and resultant magnetic properties of M_2AgF_4 (M = Na−Cs). *Inorg. Chem.* **2016**, *55*, 11479−11489.

(27) Gawraczynski, J.; Wolanski, Ł.; Grzelak, A.; Mazej, Z.; Struzhkin, V.; Grochala, W. Phase transitions and amorphization of M_2AgF_4 (M = Na, K, Rb) compounds at high pressure. *Crystals* **2022**, *12*, 458.

(28) McLain, S. E.; Dolgos, M. R.; Tennant, D. A.; Turner, J. F. C.; Barnes, T.; Proffen, T.; Sales, B. C.; Bewley, R. I. Magnetic behavior of layered Ag(II) fluorides. *Nat. Mater.* **2006**, *5*, 561−565.

(29) Dai, D.; Whangbo, M. H.; Kohler, J.; Hoch, C.; Villesuzanne, A. Electronic structure analysis of the difference between Cs_2AgF_4 and Rb_2MnF_4 in their magnetic properties and single-crystal structure determination of Rb_2MnF_4. *Chem. Mater.* **2006**, *18*, 3281−3286.

(30) Lancaster, T.; Blundell, S. J.; Baker, P. J.; Hayes, W.; Giblin, S. R.; McLain, S. E.; Pratt, F. L.; Salman, Z.; Jacobs, E. A.; Turner, J. F. C.; et al. Intrinsic magnetic order in Cs_2AgF_4 detected by muon-spin relaxation. *Phys. Rev. B* **2007**, *75*, No. 220408.

(31) Tong, J.; Kremer, R. K.; Köhler, J.; Simon, A.; Lee, C.; Kan, E.; Whangbo, M.-H. The layered ferromagnet Cs_2AgF_4: antiferromagnetic inter-layer coupling driven by magnetic dipole-dipole interactions. *Z. Kristallogr.* **2010**, *225*, 498−503.

(32) Lee, C.; Shim, J. H.; Whangbo, M. H. Cause for the orbital ordering of Cs_2AgF_4 and its effect on thermoelectric properties. *Inorg. Chem.* **2018**, *57*, 11895−11900.
(33) Hao, X.; Xu, Y.; Wu, Z.; Zhou, D.; Liu, X.; Meng, J. Orbital ordering in Cs_2AgF_4 from first principles. *Phys. Rev. B* **2007**, *76*, No. 054426.
(34) Kan, E.; Yuan, L.-F.; Yang, J.; Hou, J. G. First-principles calculations of the electronic and magnetic properties of Cs_2AgF_4. *Phys. Rev. B* **2007**, *76*, No. 024417.
(35) Wu, H.; Khomskii, D. I. Orbital ordering in the ferromagnetic insulator Cs_2AgF_4 from first principles. *Phys. Rev. B* **2007**, *76*, No. 155115.
(36) Kasinathan, D.; Koepernik, K.; Nitzsche, U.; Rosner, H. Ferromagnetism induced by orbital order in the charge-transfer insulator Cs_2AgF_4: an electronic structure study. *Phys. Rev. Lett.* **2007**, *99*, No. 247210.
(37) de Jongh, L. J.; Miedema, A. R. Experiments on simple magnetic model systems. *Adv. Phys.* **1974**, *23*, 1−260.
(38) de Jongh, L. J.; Block, R. On the exchange interactions in some 3d-Metal ionic compounds. *Physica B+C* **1975**, *79*, 568−593.
(39) Aramburu, J. A.; Bhowmik, A.; García-Lastra, J. M.; García-Fernández, P.; Moreno, M. Insight into compounds with $Cu(H_2O)_6^{2+}$ units: new ideas for understanding Cu^{2+} in Tutton salts. *J. Phys. Chem. C* **2019**, *123*, 3088−3101.
(40) Aramburu, J. A.; García-Fernández, P.; García-Lastra, J. M.; Barriuso, M. T.; Moreno, M. Colour due to Cr^{3+} Ions in oxides: a study of the model system $MgO:Cr^{3+}$. *J. Phys.: Condens. Matter* **2013**, *25*, No. 175501.
(41) García-Lastra, J. M.; Aramburu, J. A.; Barriuso, M. T.; Moreno, M. Impurities in noncubic crystals: stabilization mechanisms for Jahn-Teller Ions in layered perovskites. *Phys. Rev. Lett.* **2004**, *93*, No. 226402.
(42) Aramburu, J. A.; García-Lastra, J. M.; García-Fernández, P.; Barriuso, M. T.; Moreno, M. Cu^{2+} in layered compounds: origin of the compressed geometry in the model system $K_2ZnF_4:Cu^{2+}$. *Inorg. Chem.* **2013**, *52*, 6923−6933.
(43) Friebel, C.; Reinen, D. Ligandenfeld- und ESR-spektroskopische untersuchungen zum Jahn-Teller-effekt des Ag^{2+}-lons in fluoridischer koordination. *Z. anorg. allg. Chem.* **1976**, *413*, 51−60.
(44) Tong, J.; Köhler, J.; Simon, A.; Lee, C.; Whangbo, M.-H. Optical properties of the orchid colored silver(II) fluoride Cs_2AgF_4. *Z. Anorg. Allg. Chem.* **2012**, *638*, 1792−1795.
(45) Kohn, W.; Sham, L. J. Self-consistent equations including exchange and correlation effects. *Phys. Rev.* **1965**, *140*, A1133−A1138.
(46) Dovesi, R.; Saunders, V. R.; Roetti, C.; Orlando, R.; Zicovich-Wilson, C. M. *CRYSTAL17 user's manual*; University of Torino, Torino, 2017.
(47) *Crystal web site*. https://www.crystal.unito.it (accessed 2023-02-15).
(48) Aramburu, J. A.; Moreno, M. Understanding the structure and ground state of the prototype CuF_2 compound not due to the Jahn−Teller effect. *Inorg. Chem.* **2019**, *58*, 4609−4618.
(49) Aramburu, J. A.; Moreno, M. Explaining the optical spectrum of CrF_2 and CuF_2 model materials: role of the tetragonal to monoclinic instability. *Phys. Chem. Chem. Phys.* **2019**, *21*, 11714−11723.
(50) Sánchez-Movellán, I.; Moreno-Ceballos, J.; García-Fernández, P.; Aramburu, J. A.; Moreno, M. New ideas for understanding the structure and magnetism in AgF_2: Prediction of ferroelasticity. *Chem. − Eur. J.* **2021**, *27*, 13582−13590.
(51) Peintinger, M. F.; Oliveira, D. F.; Bredow, T. J. Consistent Gaussian basis sets of triple-zeta valence with polarization quality for solid-state calculations. *J. Comput. Chem.* **2013**, *34*, 451−459.
(52) *Crystal basis sets*. https://www.crystal.unito.it/basis-sets.php(accessed 2023-03-04).
(53) Bredow, T.; Gerson, A. R. Effect of exchange and correlation on bulk properties of MgO, NiO, and CoO. *Phys. Rev. B* **2000**, *61*, 5194−5201.
(54) te Velde, G.; Bickelhaupt, F. M.; Baerends, E. J.; Guerra, C. F.; van Gisbergen, S. J. A. Chemistry with ADF. *J. Comput. Chem.* **2001**, *22*, 931−967.
(55) Moreno, M; Aramburu, J. A.; Barriuso, M. T. Electronic properties and bonding in transition metal complexes: influence of pressure. In *Optical spectra and chemical bonding in inorganic compounds. Structure and bonding*; Mingos, D. M. P.; Schönherr, T., Eds.; Springer: Berlin, Heidelberg, 2004; pp. 127−152.
(56) Colaneri, M. J.; Vitali, J. Effect of the lattice field on the electronic structure and dynamics of copper−hexahydrate in Tutton salts. *J. Phys. Chem. A* **2021**, *125*, 3268−3278.
(57) Van Gool, W.; Piken, A. G. Lattice self-potentials and Madelung constants for some compounds. *J. Mater. Sci.* **1969**, *4*, 95−104.
(58) Tosi, M. P. Cohesion of ionic solids in the Born model. *Solid State Phys.* **1964**, *16*, 1−120.
(59) Owen, J.; Harris, E.A. Pair spectra and exchange interactions. In *Electron Paramagnetic Resonance*; Geschwind, S., Ed.; Plenum: New York, 1972.
(60) Ham, F. S. Jahn-Teller effects in Electron Paramagnetic Resonance spectra. In *Electron Paramagnetic Resonance*; Geschwind, S., Ed.; Plenum: New York, 1972 pp. 1−119.
(61) García-Fernández, P.; Trueba, A.; Barriuso, M. T.; Aramburu, J. A.; Moreno, M. Tunneling splitting of Jahn-Teller ions in oxides. *Phys. Rev. Lett.* **2010**, *104*, No. 035901.
(62) García-Fernández, P.; Trueba, A.; Barriuso, M. T.; Aramburu, J. A.; Moreno, M. Dynamic and static Jahn-Teller effect in impurities: determination of the tunneling splitting. *Prog. Theor. Chem. Phys.* **2011**, *23*, 105−142.
(63) Minner, E.; Lovy, D.; Bill, H. Electron-Paramagnetic-Resonance and relaxation study of copper(II) and silver(II) In $CsCdF_3$ single-crystals. *J. Chem. Phys.* **1993**, *99*, 6378−6383.
(64) García-Fernández, P.; Barriuso, M. T.; Garcia-Lastra, J. M.; Moreno, M.; Aramburu, J. A. Compounds containing tetragonal Cu^{2+} complexes: is the d_{x2-y2}-d_{3z2-r2} gap a direct reflection of the distortion? *J. Phys. Chem. Lett.* **2013**, *4*, 2385−2390.
(65) Low, W.; Suss, J. T. Jahn-Teller effect of Ni^+ and Cu^{2+} in single crystals of calcium oxide. *Phys. Lett.* **1963**, *7*, 310−312.
(66) Aramburu, J. A.; García-Fernández, P.; García-Lastra, J. M.; Moreno, M. A genuine Jahn-Teller system with compressed geometry and quantum effects originating from zero-point motion. *Chem. Phys. Chem.* **2016**, *17*, 2146−2156.
(67) Sánchez-Movellán, I.; Aramburu, J. A.; Moreno, M. Local structure and excitations in systems with CuF_6^{4-} units: lack of Jahn−Teller effect in the low symmetry compound Na_2CuF_4. *Phys. Chem. Chem. Phys.* **2020**, *22*, 7875−7887.
(68) Reinen, D. The modulation of Jahn−Teller coupling by elastic and binding strain perturbations: a novel view on an old phenomenon and examples from solid-state chemistry. *Inorg. Chem.* **2012**, *51*, 4458−4472.
(69) Bersuker, I. B.; Gorinchoi, N. N.; Polinger, V. Z. On the origin of dynamic instability of molecular systems. *Theor. Chim. Acta* **1984**, *66*, 161−172.
(70) García-Fernández, P.; García-Lastra, J. M.; Trueba, A.; Barriuso, M. T.; Aramburu, J. A.; Moreno, M. Insulators containing $CuCl_4X_2^{2-}$ (X = H_2O, NH_3) units: origin of the orthorhombic distortion observed only for $CuCl_4(H_2O)_2^{2-}$. *Phys. Rev. B: Condens. Matter Mater. Phys.* **2012**, *85*, No. 094110.
(71) Borcherts, R. H.; Kanzaki, H.; Abe, H. EPR spectrum of a Jahn-Teller system, $NaCl:Cu^{2+}$. *Phys. Rev. B* **1970**, *2*, 23−27.
(72) Valiente, R.; Lezama, L. M.; Rodríguez, F.; Moreno, M. Study of bidimensional $(CH_3NH_3)_2CdCl_4:Cu^{2+}$ and $(CH_3NH_3)_2CuCl_4$. *Mater. Sci. Forum* **1997**, *239*, 729−732.
(73) Riley, M. J.; Hitchman, M. A.; Reinen, D. Effects of vibronic coupling on the EPR spectra of copper(II) doped K_2ZnF_4. *Chem. Phys.* **1986**, *102*, 11−28.
(74) Abragam, A.; Bleaney, B. *Electron paramagnetic resonance of transition Ions*; Clarendon Press: Oxford, 1970; pp. 461.

https://doi.org/10.1021/acs.jpcc.3c03895
J. Phys. Chem. C 2023, 127, 16695−16708

(75) Boettcher, F.; Spaeth, J. M. ENDOR investigation of Cu^{2+} centres in NH_4Cl. *Phys. Status Solidi B* **1974**, *61*, 465−473.
(76) Valiente, R.; Aramburu, J. A.; Barriuso, M. T.; Moreno, M. Electronic structure of Ag^{2+} impurities in halide lattices. *J. Phys.: Condens. Matter* **1994**, *6*, 4515−4525.
(77) Anderson, P. W. Theory of magnetic exchange interactions: exchange in insulators and semiconductors. *Solid State Phys.* **1963**, *14*, 99−214.
(78) Owen, J.; Thornley, J. H. Covalent bonding and magnetic properties of transition metal ions. *Rep. Prog. Phys.* **1966**, *29*, 675.
(79) Hay, P. J.; Thibeault, J. C.; Hoffmann, R. Orbital interactions in metal dimer complexes. *J. Am. Chem. Soc.* **1975**, *97*, 4884−4899.
(80) Kugel, K.; Khomskiĭ, D. I. The Jahn-Teller effect and magnetism: transition metal compounds. *Phys.-Usp.* **1982**, *25*, 621−664.
(81) Kugel, K.; Khomskiĭ, D. I. Orbital and magnetic structure of two-dimensional ferromagnets with Jahn-Teller ions. *Solid State Commun.* **1973**, *13*, 763−766.
(82) Sugano, S.; Tanabe, Y.; Kamimura, H. *Multiplets of transition-metal ions in crystals; Academic Press*: New York, 1970; pp. 263−270, 126−153.
(83) Larsson, S.; Connolly, J. W. D. Spin and bonding properties and optical spectra of octahedral transition metal complexes using the multiple scattering Xα method. *J. Chem. Phys.* **1974**, *60*, 1514−1521.
(84) Adachi, H.; Shiokawa, S.; Tsukada, M.; Satoko, C.; Sugano, S. Discrete variational Xα cluster calculations. III. Application to transition metal complexes. *J. Phys. Soc. Jpn.* **1979**, *47*, 1528−1537.
(85) Jeck, R. K.; Krebs, J. J. First and second-shell hyperfine interactions in iron-group-doped perovskite fluorides. *Phys. Rev. B* **1972**, *5*, 1677−1687.
(86) Simonetti, J.; McClure, D. S. Electron transfer bands of the divalent 3d series ions in LiCl. *J. Chem. Phys.* **1979**, *71*, 793−801.
(87) Moreno, M.; Aramburu, J. A.; Barriuso, M. T. Ni^{+} in fluoride lattices: a 3d → 4p transition in the near-ultraviolet region. *J. Phys. C: Solid State Phys.* **1986**, *19*, L315−L319.
(88) Stanley, H. E.; Kaplan, T. A. Possibility of a phase transition for the two-dimensional Heisenberg model. *Phys. Rev. Lett.* **1966**, *17*, 913−915.
(89) Hagen, S. H.; Trappeniers, N. J. ESR of copper complexes in NH_4Cl, ND_4Cl and CsCl. *Physica* **1970**, *47*, 165−181.
(90) Breñosa, A. G.; Moreno, M.; Rodríguez, F.; Couzi, M. Evidence for anomalous relaxation of the $CuCl_4(NH_3)_2^{2-}$ center in NH_4Cl below Tc. *Phys. Rev. B* **1991**, *44*, 9859−9863.
(91) Soethe, H.; Vetrov, V. A.; Spaeth, J. M. Local instability of The MnF_8 complex in BaF_2:Mn^{2+} studied by ENDOR. *J. Phys.: Condens. Matter* **1992**, *4*, 7927−7936.
(92) García Fernández, P.; Aramburu, J. A.; Barriuso, M. T.; Moreno, M. Local symmetry change in BaF_2:Mn^{2+} at ∼50 K: microscopic insight. *J. Chem. Phys.* **2008**, *128*, No. 124513.
(93) Kurzydłowski, D.; Derzsi, M.; Mazejc, Z.; Grochala, W. Crystal, electronic, and magnetic structures of M_2AgF_4 (M = Na-Cs) phases as viewed from the DFT+U method. *Dalton Trans.* **2016**, *45*, 16255−16261.
(94) Grochala, W. Small changes, big consequences. *Nat. Mater.* **2006**, *5*, 513−514.
(95) García Fernández, P.; Aramburu, J. A.; Barriuso, M. T.; Moreno, M. Cu^{2+} impurities in fluorite-type crystals: mechanisms favoring an off-center motion. *Phys. Rev. B* **2004**, *69*, No. 174110.
(96) Roelfsema, K. E.; Den Hartog, H. W. Electric field effect of EPR spectra of cubic impurities in $SrCl_2$. *J. Magnetic Resonance* **1978**, *29*, 255−273.
(97) García-Lastra, J. M.; García-Fernández, P.; Calle-Vallejo, F.; Trueba, A.; Aramburu, J. A.; Moreno, M. Quantifying local and cooperative components in the ferroelectric distortion of $BaTiO_3$: learning from the off-center motion in the $MnCl_6^{5-}$ complex formed in KCl:Mn^{+}. *Inorg. Chem.* **2014**, *53*, 6534−6543.
(98) Gǎzo, J.; Bersuker, I. B.; Garaj, J.; Kabesova, M.; Kohout, J.; Langfelderova, H.; Melnik, M.; Serator, M.; Valach, F. Plasticity of coordination sphere of copper(II) complexes, its manifestation and causes. *Coord. Chem. Rev.* **1976**, *19*, 253−297.
(99) Gawraczyński, J.; Kurzydłowski, D.; Ewings, R. A.; Bandaru, S.; Gadomski, W.; Mazej, Z.; Ruani, G.; Bergenti, I.; Jaroń, T.; Ozarowski, A.; et al. Silver route to cuprate analogs. *Proc. Natl. Acad. Sci. U. S. A.* **2019**, *116*, 1495−1500.
(100) Mazej, Z.; Goreshnik, E.; Jagličić, Z.; Gaweł, B.; Łasocha, W.; Grzybowska, D.; Jarón, T.; Kurzydłowski, D.; Malinowski, P.; Koźminski, W.; et al. $KAgF_3$, K_2AgF_4 and $K_3Ag_2F_7$: important steps towards a layered antiferromagnetic fluoroargentate(II). *CrystEngComm* **2009**, *11*, 1702−1710.

https://doi.org/10.1021/acs.jpcc.3c03895
J. Phys. Chem. C 2023, 127, 16695−16708